Master's Thesis

Development on hybrid-capacitor with high energy density

Seong-Ji Ha

Department of Energy Engineering

(Energy Engineering)

Graduate School of UNIST

2019

Development on hybrid-capacitor with high energy density

Seong-Ji Ha

Department of Energy Engineering

(Energy Engineering)

Graduate School of UNIST

Development on hybrid-capacitor with energy density

A thesis/dissertation
submitted to the Graduate School of UNIST
in partial fulfillment of the
requirements for the degree of
Master of Science

Seong-Ji Ha

12. 05. 2018
Approved by

Advisor
Ji-Hyun Jang

Development on hybrid-capacitor with high energy density

Seong-Ji Ha

This certifies that the thesis/dissertation of Seong-Ji Ha is approved

12. 05. 2018

signature

Advisor: Ji-Hyun Jang

signature

Jongnam Park

signature

Hyun-Kon Song

Table of contents

List of Figures

List of Tables

Abstracts

In this thesis, I observe the methods to overcome the low energy density in the supercapacitor system which is the crucial issue in energy storage industries. I challenge simple and easy approaches to achieve better capacitor properties than before by fabricating the three-dimensional structure of current collector and colloid structure of active material. First, rational design of the current collector with large surface area and high electrical conductivity is the very important factor in the hybrid-capacitor system for high performance. Nickel particles-coated three-dimensional graphene foam current collector (Ni-GF) was fabricated by two simple steps from cost-effective commercial cotton and nickel chloride, based on the growth of graphene on the surface of nickel particles. The welded nickel particles on graphene sheets and three-dimensional graphene networks enhance the electrical conductivity and various pores in graphitic carbon domains gives the high surface area, generated by the thermal decomposition of organic precursors during a carbonization or pyrolysis process. This strategy provides the high performance in the supercapacitor system as the current collector. The high surface area of Ni-GF supports a lot of reaction sites of active materials and high electrical conductivity helps the good rate capability and long-term cycle life. The prepared $Ni(OH)_2$/Ni-GF//MnO_2/Ni-GF capacitor exhibited an excellent energy density of 175 Wh kg^{-1} at a power density of 722 W kg^{-1} for a two-electrode system.

Also, I improve the weakness of supercapacitors such as low energy density by utilizing cobalt and nickel ion colloidal electrodes on a carbonized cotton. Ni^{2+} and Co^{2+}-coated carbonized cotton (NC/CC) were prepared by simple and rapid fabrication process. The metal colloidal electrode on three-dimensional carbon foam provides many active sites, which leads to a lot of redox reactions in whole colloids of CNFs. CNFs were optimized by adjusting the contents of Co^{2+} and Ni^{2+} on carbon foams, and it showed high capacitance and stable cycle stability. The optimized NC/CC//Mn/CC capacitor leads to overcome a limitation of supercapacitor and to achieve the enhancement of capacitor properties. The outstanding performance of NC/CC//Mn/CC is attributed to the increased active sites of metal colloidal electrodes as well as to the good stability for carbon foams. These excellent electrochemical results have the great potential for energy storage devices with high values of energy density and power density.

Chapter 1. Literature review

1.1 Motivation

We use various types of energy sources such as fossil fuel oils, natural energy, and coals. Among many energy sources, there is only one difference that is renewable sources or not[1]. According to Figure 1.2, it has been used to consume energy sources in the world: Oil 33%, Coal 30%, Natural Gas 24%, Hydro 7%, Nuclear 4%, and Others 2%[2]. Among energy consumption by fuel, Renewable sources are only 6% that is Hydro and Others. Fossil fuel oils are a kind of non-renewable sources, which are confirmed that it causes our world a lot of problems such as global warming and depletion as well as that it is not abundant. Many researchers have developed substitutes to overcome a limitation of fossil fuel oils. Recently, it shows that the rapid increase in demand for electric devices using electric energy with the fast-growing electric market in Figure 1.3[3]. In the case of electric energy, it has advantages of eco-friendly, no condition to be working, and no limitation. With many advantages, it takes attention the development of various energy storage device for green energy source.

There are two types of energy storage devices which are lithium ion battery and supercapacitor. Lithium ion battery has high energy density and low self-discharge relatively, which has been mainly used in the wide range of electric device. However, lithium ion battery suffers from low safety, possibility of an explosion, and low power density compared to supercapacitor. Many electric devices need high safety, high energy density, and high stability of a long cycle to be widely used. For these reasons, supercapacitor is on the rise, which can be expected to use many electric devices. Supercapacitor takes center stage as the future energy storage system due to high power density, long cycle life, and fast charge-discharge process. There are many different properties in comparison of battery and supercapacitors (Figure 1.4 and Table 1.1)[4-5]. Power density is very important factor of energy storage system for electrical device such as electric vehicle and potable laptop. Because of this factor, I will study a supercapacitor, which has higher energy density than before.

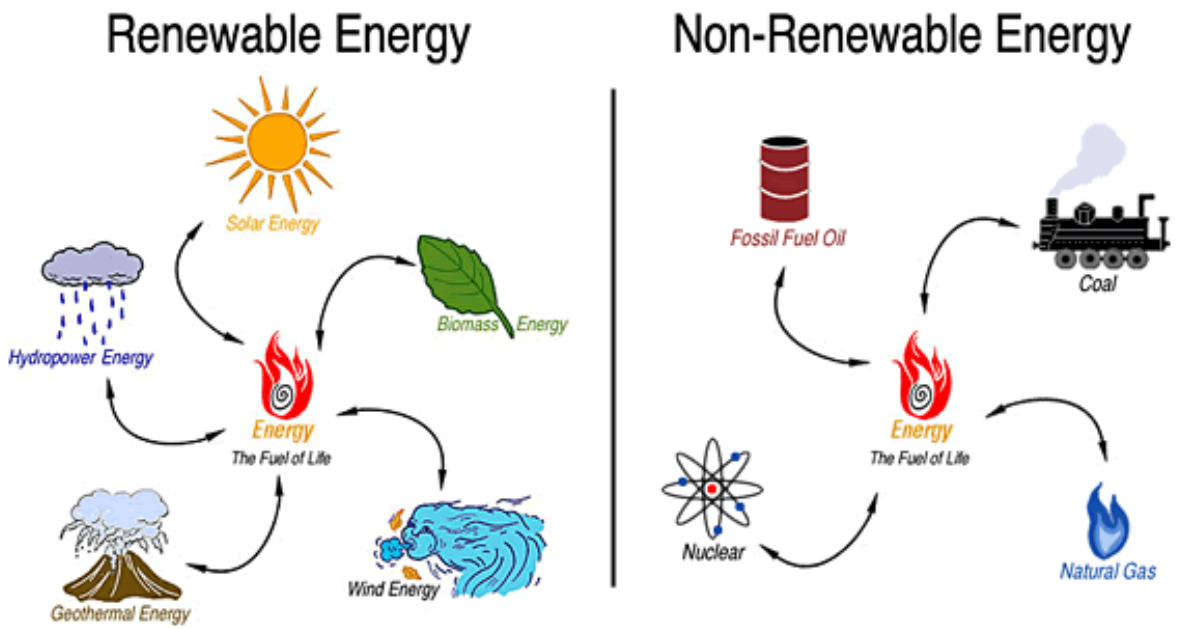

Figure 1. 1. Two categories of energy sources: renewable energy and non-renewable energy.[1]

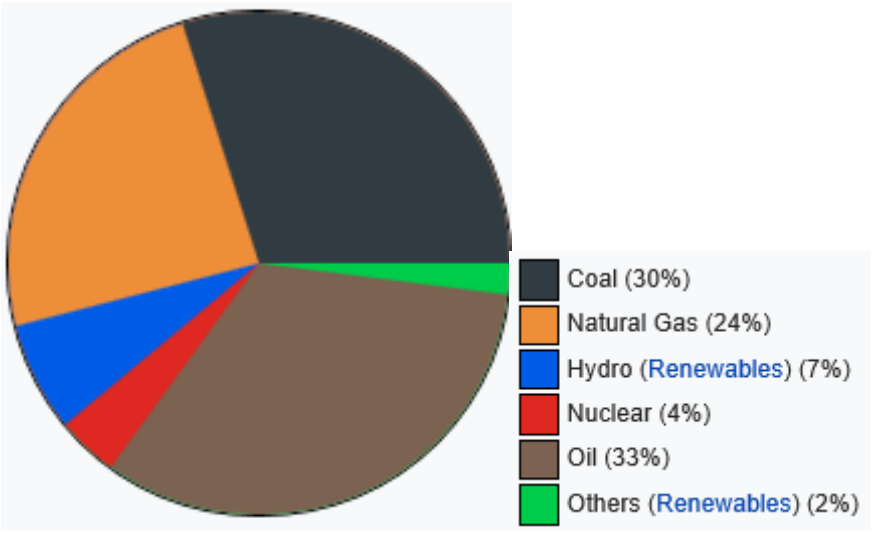

Figure 1. 2. World total primary energy consumption by fuel in 2015.[2]

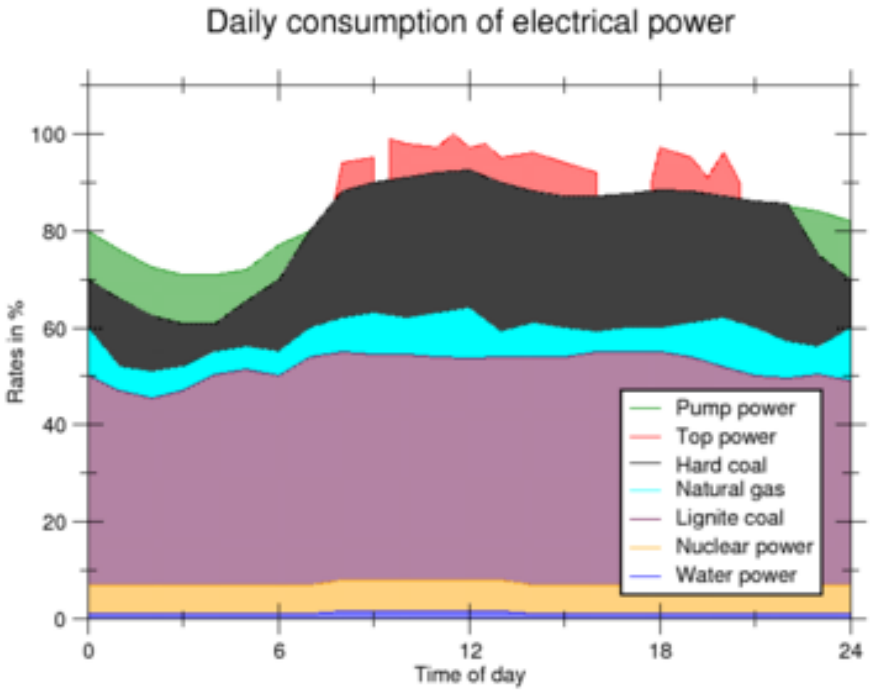

Figure 1. 3. Typical daily consumption of electrical power in Germany.[3]

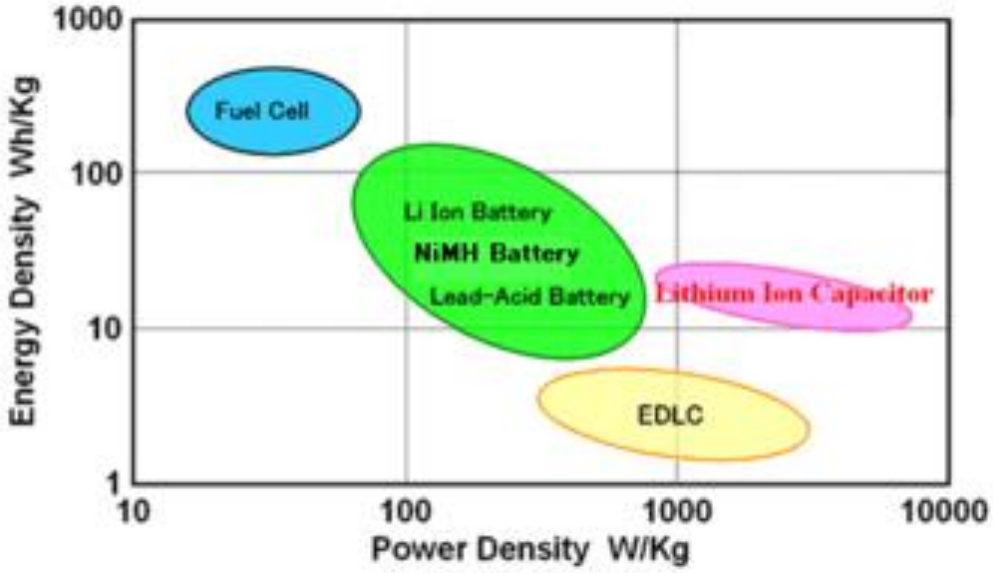

Figure 1. 4. Ragone plot of energy density vs. power density for various energy-storing devices.[4]

Table 1. 1. Comparison of the properties of battery, electrostatic capacitor and EC.[5]

	Battery	**Capacitor**	**Supercapacitor**
Discharge time	0.3–3 h	10^{-3} to 10^{-6} s	0.3–30 s
Charge time	1–5 h	10^{-3} to 10^{-6} s	0.3–30 s
Energy density (Wh/kg)	10–100	<0.1	1–10
Specific power (W/kg)	50–200	>10,000	≈1000
Charge-discharge efficiency	0.7–0.85	≈1	0.85–0.98
Cycle life	500–2000	>500,000	>100,000

1.2 Capacitor : electrochemical energy storage

Supercapacitor is composed of a positive electrode, a negative electrode, a current collector, a separator, and an electrolyte in a two electrode system (Figure 1.5). When the devices were charged, the positive electrode and the negative electrode attracted reverse ions. It caused charge separation on the each electrodes. As a result, the surface of the two electrodes was stored up positively charged ions and negatively charged ions. Based on the storage principle, the supercapacitors are classified into three categories: Electrical double-Layer capacitors (EDLCs)[6], pseudo-capacitors[7], and hybrid capacitors[8]. There are a difference that is method of storing up charges. EDLCs store the charges by physically static forces that works on the surface of electrode. In the case of pseudo-capacitors, the charges are achieved by faradaic electron transfer with chemically reversible redox reaction. In the case of hybrid capacitors, it has been increasing attracted due to using electrodes with one exhibiting mostly electrostatic capacitance and the other mostly electrochemical capacitance, like the lithium ion capacitors.

1.2.1 Electrical Double-Layer Capacitors (EDLCs)

For the first time, the studies of supercapacitor were focused on the only electrical double-layer capacitors which were called as the EDLCs. The EDLCs achieve physical ion adsorption and desorption to accumulate a lot of charges, and emerge from active materials at the electrode. Between the electrodes and the electrolyte, it can be confirmed that there is an interface. If the charge process is attained, the positively charged ions in the electrolyte move to the negative electrode, and the negatively charged ions in the electrolyte also move to the positive electrode. On the contrary, it can be put back again in the discharge process. When repeatedly applying to these processes, it can understand the working principle mechanism of the EDLCs, which are worked by physically storing electric charges for moving ions of electrolyte. It is non-faradaic reaction unlike pseudo-capacitors.

The EDLCs use the carbon-based electrodes such as activated carbon (AC)[9], graphene oxide (GO)[10], graphene[11], carbon nanotubes (CNTs)[12], and carbon aerogel[13]. Among carbon-based electrodes, graphene is the basic structural element of many other allotropes of carbon. It has many special properties: good mechanical and stability, outstanding electrical conductivity as well as high value of surface area. For these reasons, graphene is mainly used for the active materials on the supercapacitor.

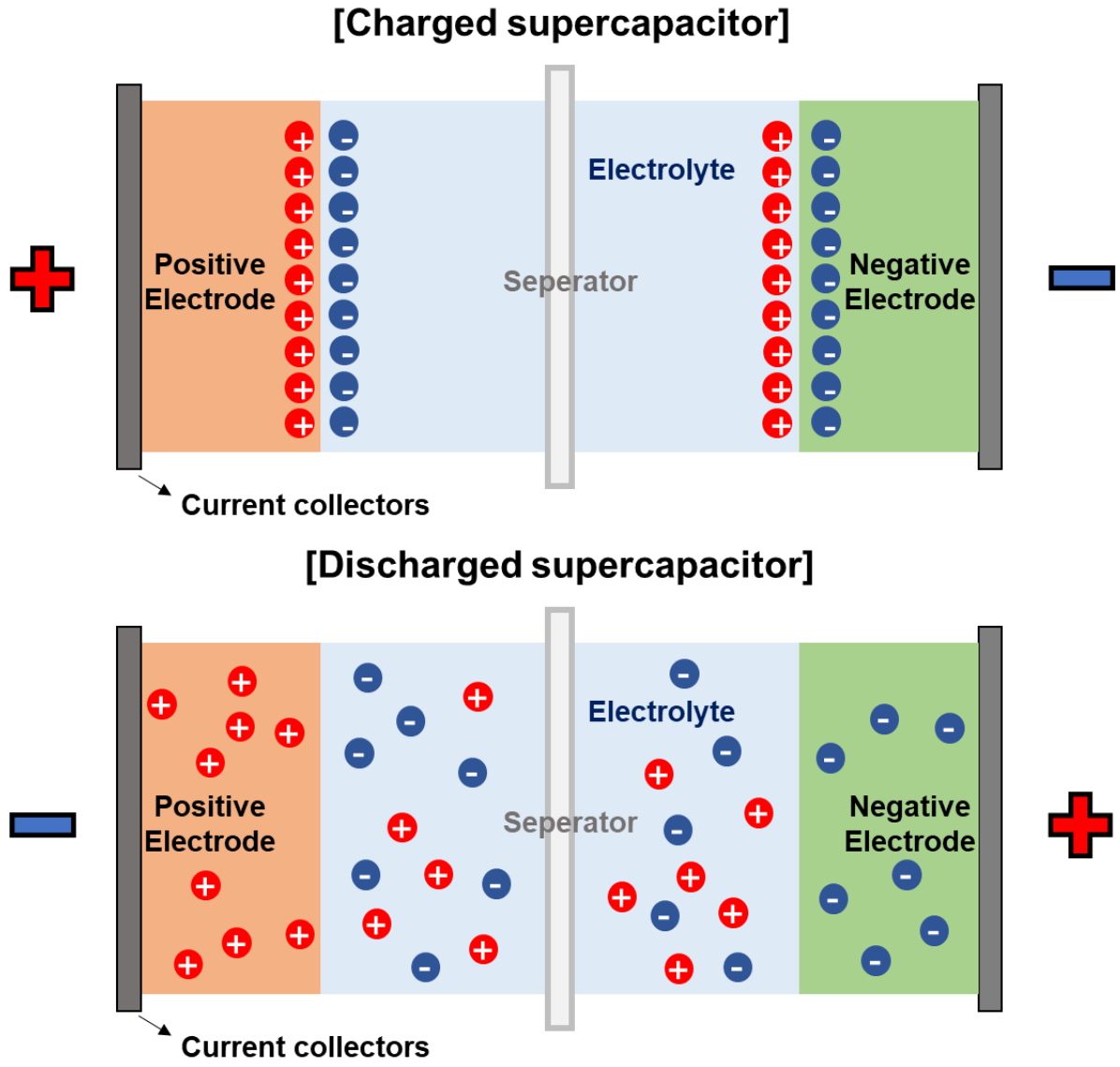

Figure 1. 5. Schematic of the mechanisms of the charged and discharged supercapacitors.

1.2.2 Pseudo-capacitors

It has been newly designing capacitors because the EDLCs has a limitation to achieve higher capacitance than before. The pseudo-capacitors are suggested to the world, which originates that it similarly works like batteries and EDLCs. The charge storage system of the pseudo-capacitors is achieved by the faradaic oxidation/reduction reactions, adsorption, or intercalation on the surface of electrodes with charge-transfer. As illustration in Figure 1.6, the protons of an electrolyte and the electrons of active materials combine to form a thick layer on the pseudo-capacitors compared to the EDLCs[14]. As a result, the EDLCs are worked by physical force, and the pseudo-capacitors are worked by redox reaction. Table 1.2 shows the more detail difference between EDLCs and pseudo-capacitors[5].

The pseudo-capacitors usually used transition metal derivatives as the active materials. Many transition metal oxides make effectively contributions to the high capacitance and the high energy density. This factor is important to attain higher capacitance for the pseudo-capacitors than the EDLCs.

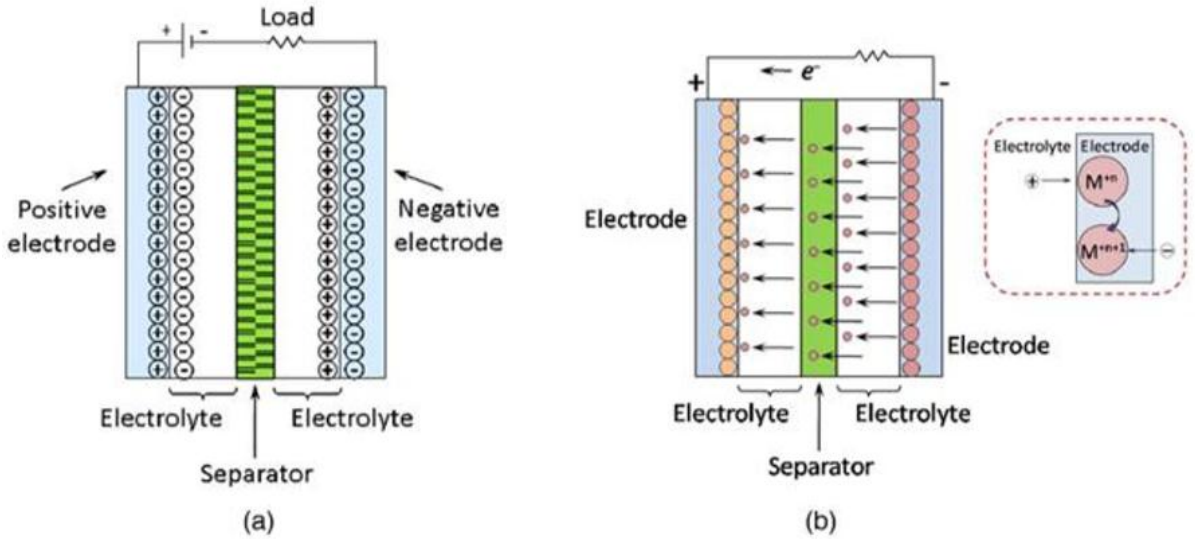

Figure 1. 6. Comparison of charge storage system about the processes of (a) electrical double-layer capacitance and (b) pseudo-capacitance.[14]

Table 1. 2. Differences of EDLC and pseudo-capacitance.[5]

	EDLC	**Pseudocapacitance**
1.	Non-faradaic	Involves faradaic process(es)
2.	20–50 μF/cm^2	2000 μF/cm^2 for single-state process; 200–500 μF/cm^2 for multi-state, overlapping processes
3.	C fairly constant with potential, except through the potential of zero charge	C fairly constant with potential for RuO_2; for single-state process, exhibits marked maximum
4.	Highly reversible charging/discharging	Can exhibit several maxima for overlapping, multi-state processes, as for H at Pt; Quite reversible but has intrinsic electrode-kinetic rate limitation determined by R_f
5.	Has restricted voltage range (contrast non-electrochemical electrostatic capacitor)	Has restricted voltage range
6.	Exhibits mirror-image voltammograms	Exhibits mirror-image voltammograms

1.3 Electrode materials for supercapacitors

1.3.1 Carbon materials

Activated carbon (AC), graphene oxide (GO), graphene, carbon nanotubes (CNTs), and carbon aerogel have one thing in common. All is a kind of carbon-based materials. Many carbon-based materials are widely used for the EDLCs due to large surface area and good conductivity. Among carbon-based materials, AC was firstly chosen for EDLC electrodes although its electrical conductivity is much lower than metal. AC can be applied to the methods of activation process: physical and chemical activation[15]. It has been produced by the heat treatment of carbonaceous raw materials at a various range of temperature (700-1200 ℃) using activating agent in the physical activation[16]. Aworn group reported that each of materials need a well-matching activating agent such as CO_2, air, steam, or a mixture of gases due to achieving the high value of surface area[17]. Nabais group prepared the physical activation of coffee endocarp in the presence of both CO_2 and steam at a temperature of 700 ℃, also discovered that the specific surface area is from 426 to 1,287 m^2g^{-1} for CO_2 activated carbons and is between 355 and 630 m^2g^{-1} [18]. Rodriguez group also suggested that there is a difference of pore size that activation process using steam is wider pores than using CO_2[19]. In the case of the chemical activation, it has been performed at a relatively low temperature (400-700 ℃) with activating agents such as NaOH, $ZnCl_2$, KOH, and $FeCl_3$[16]. It carried out carbonization and activation process together, resulting in the structure of better porosity. Zhang group performed activated carbon with the activation process using $ZnCl_2$[20]. As a result, they found out that the ratio of material and activating agent as well as temperature influence the pore structure of product and the surface area. Jin group achieved the largest specific surface area of 2959 m^2g^{-1} and high pore volume or 1.65 cm^3g^{-1} for carbon materials[21]. For these studies, AC proves that it causes improving the capacitance with the surface area, pore size distribution, and pore properties.

With the development of CNTs, it has caused an important advancement in the electrochemical field of carbon materials. CNTs have attracted attention due to their unique properties such as good mechanical, thermal stability[22], electrical property[23], and pore structure[24]. Also, there is advantages that CNTs have a lot of mesopores, in which are interconnected, resulting in a continuous charge distribution. It has been widely used as the active materials in supercapacitors with the high specific surface area (single-walled carbon nanotubes >1,600 m^2g^{-1} and multi-walled carbon nanotubes >430 m^2g^{-1})[25-26]. Pan group enhanced the surface area from 46.8 m^2g^{-1} to 109.4 m^2g^{-1} for electrochemical activation process, and achieved the increase capacitance value for three times[27]. Hata group reported the highly pure CNTs with a specific surface area of 1,300 m^2g^{-1}. They performed measurement of electrochemical performance using organic electrolyte to enlarge a range of voltage until 4 V, leading to high energy density value of 94 Wh kg^{-1} and high power density value up to 210 kW kg^{-1} [28].

Recently, it was suggested that graphene can be mainly used as an active material for supercapacitor application due to its superior characteristics of large surface area[29], high electrical conductivity[30], and chemical stability[31]. Graphene is 2D structure that consists of a one-atom thick layer in a regular hexagonal structure[32-33]. Unlike other carbon-based materials such as AC and CNTs, graphene can be worked as current collector itself. Also, graphene has higher theoretical surface area (2,630 m^2g^{-1}) than all carbon-based materials used as electrode for supercapacitor[34-35]. The capacitance value is up to 550 F g^{-1}, utilizing the entire surface of graphene electrode[30]. There are various production methods to synthesize the different types of graphene. Zhang group synthesized the three-dimensional graphene networks as a current collector for supercapacitor using the ethanol-chemical vapor deposition (CVD) method. They applied the active material of nickel oxide to the current collector, and reported high capacitance of 816 F g^{-1} [36]. Jang group fabricated a mass-producible mesoporous graphene nanoball using a precursor-assisted CVD process for supercapacitor application. They showed a specific surface area of 508 m^2g^{-1} and a mesoporous structure with a pore diameter of 4.27 nm. The supercapacitor attained a specific capacitance of 206 F g^{-1} [37]. Except for the CVD process, mechanical exfoliation, epitaxial growth, electrochemical and chemical methods, and intercalation methods in graphite are applied to synthesize graphene for supercapacitor[38-41].

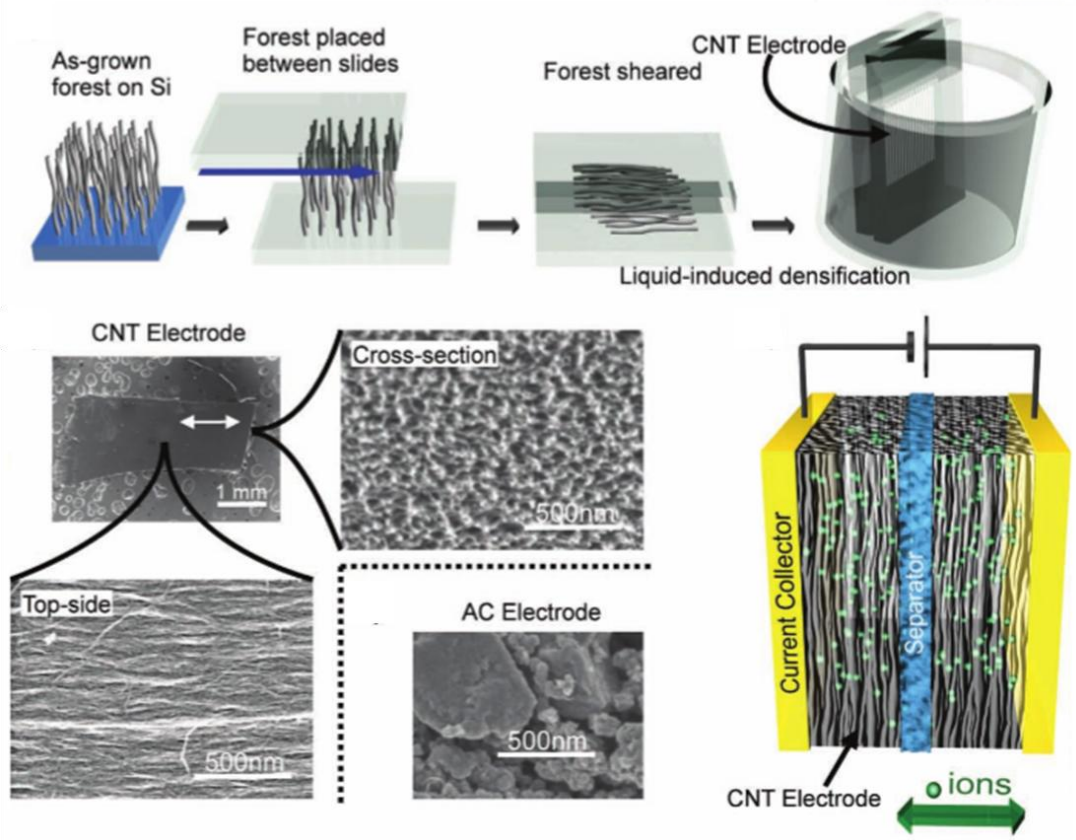

Figure 1. 7. Fabrication process and characterization of single-walled carbon nanotubes (SWNTs) electrode.[28]

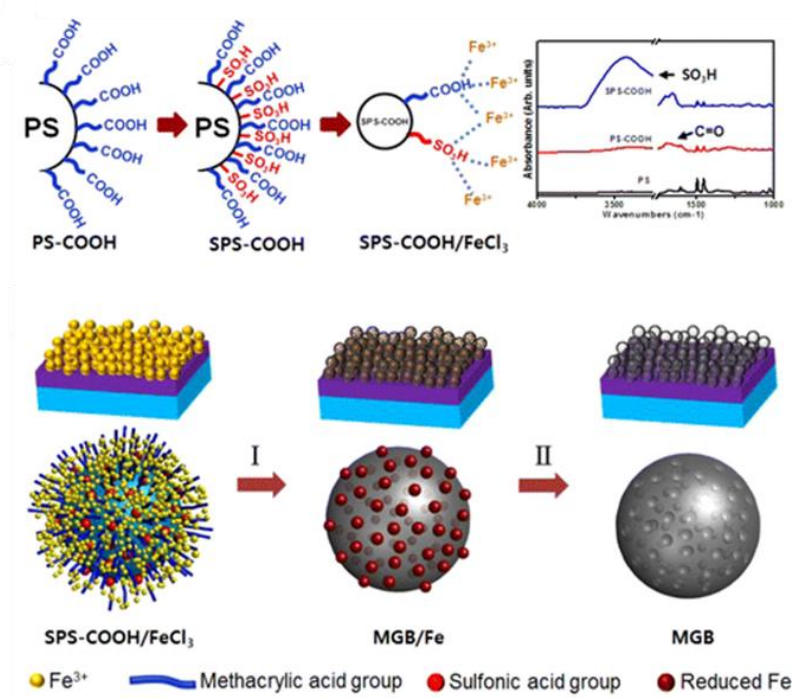

Figure 1. 8. Schematic illustration of the mesoporous graphene nanoball.[37]

1.3.2 Transition Metal oxides

Transition metal oxides are another alternative for pseudo-capacitor used as active materials due to high capacitance and high energy density. The active materials using transition metal oxides have higher value of capacitance than EDLCs about 10-100 times. Among the transition metal oxides, ruthenium dioxide (RuO_2) is the most rising active material given its advantages of wide potential window, long cycle life, high theoretical capacitance, and good conductivity[42]. However, RuO_2 is expensive as well as has a limitation applied to many applications to work in the range of 2.4 V voltage window for capacitor. Das group suggested that they introduced the electrodeposition method on the porous SWNTs film to overcome limitations. They achieved the highest capacitance value of 1,715 F g^{-1} for RuO_2-based supercapacitor, which comes close to the theoretical capacitance of 2,000 F g^{-1} [43]. RuO_2 is caused a serious problem such as environmental harmfulness despite some researchers' effort.

Nowadays manganese oxide (MnO_x) attracts a lot of interest and has special properties such as physical and chemical properties with various applications: ion exchange[44], catalysis[45], biosensor[46], energy storage[47], and molecular adsorption[48]. Tong group developed a new route to synthesize mesoporous MnO_2/carbon aerogel composites using the electrodeposition process, which is assisted by gas bubbles. They employed supercapacitor electrode, leading to high specific capacitance (515.5 F g-1) [49]. MnO_2 is mainly used for active materials for pseudo-capacitor due to its low cost, superior capacitive performance, and environmental safety.

Table 1. 3. Pseudo-capacitance and conductivity of selected metal oxides[50]

Oxide	Electrolyte	Charge storage reaction	Theoretical capacitance (F g^{-1})	Conductivity (S cm^{-1})
MnO_2	Na_2SO_4	$MnO_2 + M^+ + e^- = MMnO_2$ (M could be H^+, Li^+, Na^+, K^+)	1380 (0.9 V)	10^{-5} to 10^{-6}
NiO	KOH, NaOH	$NiO + OH^- = NiOOH + e^-$	2584 (0.5 V)	0.01–0.32
Co_3O_4	KOH, NaOH	$Co_3O_4 + OH^- + H_2O = 3CoOOH + e^-$ CoO OH + $OH^- = CoO_2 + H_2O + e^-$	3560 (0.45 V)	10^{-4} to 10^{-2}
V_2O_5	NaCl, Na_2SO_4	$V_2O_5 + 4M^+ + 4e^- = M_2V_2O_5$ (M could be H^+, Li^+, Na^+, K^+)	2120 (1 V)	10^{-4} to 10^{-2}
RuO_2, xH_2O	H_2SO_4, Na_2SO_4	$RuO_2 + xH^+ + xe^- = RuO_{2-x}$, $(OH)_x$ ($0 < x < 2$)	1200–2200 (1.23 V)	10^3 for polycrystalline, ~1 for amorphous

Table 1. 4. Summary of the transition metal oxide of electrode materials investigated.[5]

Electrode material	Electrolyte	Working voltage (V)	Specific Capacitance (F/g)
$RuO_2 \cdot H_2O$	0.5 M H_2SO_4	1.0	650
Ruthenic acid nanosheet/Au	0.5 M H_2SO_4	1.2	620
$H_{0.2}RuO_{2.1} \cdot nH_2O$	0.5 M H_2SO_4	1.2	390
RuO_2/carbon	PVA hydrogel	0.8	1000
Amorphous $Ru_{1-y}Cr_yO_2/TiO_2$	1 mol/L KOH	0.9	1272
MnO_2	0.5 M K_2SO_4	0.8	261
MnO_2/AC	0.65 M K_2SO_4	2.2	29
SnO_2/carbon aerogel	1 M H_2SO_4	1.0	68
$Ni(OH)_2$	3% KOH	0.8	578
$Ni(OH)_2$/AC	6 mol/L KOH	0.9	194
Cobalt-nickel oxides/ CNTs	1 M KOH	1.0	569
Nickel-based mischmetal/AC	BMIM-PF_6	3.0	357
Mo_2N/Ta_2O_5	3.5 mol/L H_2SO_4	0.8	106
WC/carbon	1 mol/L H_2SO_4	0.9	477
$MnFe_2O_4$	1 M $LiPF_6$ + EC/EMC	2.5	126
TiN	1 M KOH	0.2	238
V_2O_5	2 M KCl	0.7	262

1.4 References

1. Martinot, E.; Sawin, J. L., What is a Renewable Energy Source?. *SOLAR ENERGY* **2013,** *5*.
2. Aleklett, K.; Campbell, C. J., Statistical Review of World Energy-overview. *Statistical Review of World Energy* **2016,** 6.
3. Markus Scheweiss, Electricity sector in Germany. *Rheinisch-Westfalisches Elecktrizitatswerk* **2005**.
4. Christen, Thomas; Carlen, Martin W., Theory of Ragone plots *Journal of Power sources* **2000,** *91* (2), 210-216.
5. Zhang, Y.; Feng, H.; Wu, X.; Wang, L.; Zhang, A.; Xia, T.; Dong, H.; Li, X.; Zhang, L., Progress of electrochemical capacitor electrode materials: A review. *International journal of hydrogen energy* **2009,** *34* (11), 4889-4899.
6. Pandolfo A.G.; Hollenkamp A.F., Carbon properties and their role in supercapacitors. *J. Power Sources* **2006,** *157* (1), 11-27.
7. Mathieu Toupin, Thierry Brousse, and Daniel Belanger, Charge Storage Mechanism of MnO_2 electrode Used in Aqueous Electrochemical Capacitor. *Chem. Mater.* **2004,** *16* (16), 3184-3190.
8. Volfkovich Yu.M.; Mikhailin A.A.; Bograchev D.A.; Sosenkin V.E.; Bagotsky V.S., Studies of Supercapacitor Carbon Electrodes with High Pseudocapacitance. *Recent Trend in Electrochemical Science and Technology* **2012,** *7*, 159-182.
9. Jorge Laine, Simon Yunes, Effect of the preparation method on the pore size distribution of activated carbon from coconut shell. *Carbon* **1992,** *30* (4), 601-604.
10. Elzbieta Frackowiak, Francois Beguin, Carbon materials for the electrochemical storage of energy in capacitors. *Carbon* **2001,** *39* (6), 937-950.
11. Maher F. El-Kady, Veronica Strong, Sergey Dubin, Richard B. Kaner, Laser Scribing of High-Performance and Flexible Graphene-Based Electrochemical Capacitors. *Science* **2012,** *335* (6074), 1326-1330.
12. Xin Li, Jiepeng Rong, Bingqing Wei, Electrochemical Behavior of Single-Walled Carbon Nanotube Supercapacitors under Compressive Stress. *ACS Nano* **2010,** *4* (10), 6039-6049.
13. Fisher U.; Saliger R.; Bock V.; Petricevic R.; Fricke J., Carbon Aerogels as Electrode Material in Supercapacitors. *J. Porous Mat.* **1997,** *4* (4), 281-285.
14. Vangari M.; Pryor T.; Jiang L., Supercapacitors: Review of Materials and Fabrication Methods. *J.Energy Eng.* **2013,** *139* (2), 72-79.
15. A.M. Abioye, F.N. Ani, Studies of activated carbons used in double-layer capacitors. *Renewable and Sustainable Energy Reviws* **2015,** *52*, 1282-1293.
16. A.G. Pandolfo and A.F. Hollenkamp., Caron properties and their role in supercapaitors. *J. Power*

Sources **2006,** *157* (1), 11-27.

17. Aworn A, Thiravetyan P, Nakbanpote W., Preparation and characteristics of agricultural waste activated carbon by phisical activation micro- and mesopores. *J. Anal. Appl. Pyrolysis* **2008,** *82*, 279-285.
18. Nabais JMV, Nunes P, Carrott PJM, Ribeiro Carrott MML, Garcia AM, Diaz-Diez MA., Production of activated carbons from coffee endocarp by CO^2 and steam activation. *Fuel Process Technol* **2008,** *89*, 262-268.
19. F. Rodriguez-Reinoso, H. Marsh, E.A. Heintz., Introduction to Carbon Technologies. *Universidad de Alicante* **1997,** *chap.2*.
20. Zhang J, Gong L, Sun K, Jiang J, Zhang X., Preparation of activated carbon from waste Camellia oleifera shell for supercapacitor application. *J. Solid State Electrochem.* **2011,** *275*, 302-305.
21. Jin H, Wang X, Gu Z, Polin J., Carbon materials from high ash biochar for supercapacitor and improvement of capacitance with HNO_3 surface oxidation. *J. Power Sources* **2013,** *236*, 285-292.
22. Q. Cheng, J. Tang, J. Ma, H. Zhang, N. Shinya and L. C. Qin., Graphene and carbon nanotube composite electrodes for supercapacitors with ultra-high energy density. *Phys. Chem. Chem. Phys.* **2011,** *13* (7), 17615-17624.
23. P. Tamilarasan, A.K. Mishra and S. Ramaprabhu., Graphene/ionic liquid binary electrode material for high performance supercapacitor. *IEEE* **2011**.
24. C. Du and N. Pan., Carbon Nanotube-Based Supercapacitors. *Nanotech. Law & Business* **2007,** *4* (1), 569-576.
25. Martin Cinke, Jing Li, Bin Chen, Alan Cassell, Lance Delzeit, Jie Han, M. Meyyappan, Pore structure of raw and purified HiPco single-walled carbon nanotubes. *Chem. Phys. Lett. 365* **2002,** *365*, 69-74.
26. Chunming Niu, Enid K. Sichel, Robert Hoch, David Moy, and Howard Tennent, High power electrochemical capacitors based on carbon nanotube electrodes. *Appl. Phys. Lett. 70* **1997,** *70* (5), 1480-1482.
27. Pan H., Poh C.K., Feng Y.P., and Jianyi Lin, Supercapacitor electrodes from tubes-in-tube carbon nanostructures. *Chem. Mater.* **2007,** *19* (25), 6120-6125.
28. Ali Izadi-Najafabadi, Satoshi Yasuda, Kazufumi Kobashi, Takeo Yamada, Don N. Futaba, Hiroaki Hatori, Motoo Yumura, Sumio Iijima, Kenji Hata, Extracting the full potential of single-walled carbon nanotubes as durable supercapacitor electrodes operable at 4 V with high power and energy density. *Adv. Mater.* **2010,** *22*, E235-E241.
29. H. Wang, Q. Hao and X. Yang, Graphene oxide doped polyaniline for supercapacitors. *Electrochem. Commun.* **2009,** *11*, 1158-1161.
30. C. Liu, Z. Yu, D. Neff, A. Zhamu and B. Z. Jang, Graphene-Based Supercapacitor with an

Ultrahigh Energy Density *Nano lett.* **2010,** *10* (12), 4863-4868.

31. Ezzat G. Bakhoum, Marvin H. M. Cheng, Novel Capacitive Pressure Sensor. *IEEE* **2010,** *49*, 443-450.
32. Palaniselvam, Thangavelu; Baek, Jong-Beom, Graphene based 2D-materials for supercapacitors. *2D Materials* **2015,** *2*, 032002.
33. Yoo, J. J.; Balakrishnan, K.; Huang, J.; Meunier, V.; Sumpter, B. G.; Srivastava, A.; Conway, M.; Reddy, A. L. M.; Yu, J.; Vajtai, R.; Ajayan, P.M., Ultrathin planar graphene supercapacitors. *Nano Lett.* **2011,** *11* (4), 1423-1427.
34. T. Y. Kim, H. W. Lee, M. Stoller, D. R. Dreyer, C. W. Bielawski, R. S. Ruoff and K. S. Suh, High-performance Supercapacitors Based on Poly(ionic liquid)-Modified Graphene Electrodes. *ACS nano* **2011,** *5* (1), 436-442.
35. K. Moon, Z. Li, Y. Yao, Z. Lin, Q. Liang, J. Agar, M. Song, M. Liu and C.P. Wong, Graphene for ultracapacitors. *IEEE* **2010,** 1323-1328.
36. Cao, X.; Shi, Y.; Shi, W.; Lu, G.; Huang, X.; Yan, Q.; Zhang, Q.; Zhang, H., Preparation of novel 3D graphene networks for supercapacitor applications. *Small* **2011,** *7* (22), 3163-3168.
37. Lee, J.-S.; Kim, S.-I.; Yoon, J.-C.; Jang, J.-H., Chemical vapor deposition of mesoporous graphene nanoballs for supercapacitor. *ACS nano* **2013,** *7* (7), 6047-6055.
38. R. Ramachandran, V. Mani, S.M. Chen, R. Saraswathi and B.S. Lou, Recent Trends in Graphene based Electrode Materials for Energy Storage Devices and Sensors Applications. *Int. J. Electrochem. Sci.* **2013,** *8*, 11680-11694.
39. R. Ramachandran, M. Saranyam V. Velmurugan, B.P.C. Raghupathy, S.K. Jeong and A.N. Grace, Effect of reducing agent on graphene synthesis and its influence on charge storage towards supercapacitor applications. *Applied Energy* **2015,** *153*, 22-31.
40. Yanyun Liu, Dong Zhang, Yu Shang, Chao Guo, A simple and efficient electrochemical reductive method for graphene oxide. *Bull. Mater. Sci.,* **2014,** *37* (6), 1529-1533.
41. T. Kuilla, S. Bhadra, D. Yao, N.H. Kim, S. Bose and J. H. Lee, Recent Advances in Graphene Based Polymer Composites. *Progress Polymer Sci.* **2010,** *35* (11), 1350-1375.
42. Kim, I.-H.; Kim, K.-B., Electrochemical characterization of hydrous ruthenium oxide thin-film electrodes for electrochemical capacitor applications. *Journal of The Electrochemical Society* **2006,** *153* (2), A383-A389.
43. Rajib K. Das, Bo Liu, John R. Reynolds and Andrew G. Rinzler, Engineered Macroporosity in Single-Wall Carbon Nanotube Films. *Nano Lett.* **2009,** *9* (2), 677-683.
44. H. Xia, Y. Wang, J. Lin and L. Lu, Hydrothermal synthesis of MnO_2/CNT nanocomposite with CNT core/porous MnO2 sheath hierarchy architecture for supercapacitors. *Nanoscale Res. Lett.* **2012,** *7* (1), 33.

45. I. Acznik, K. Lota, A. Sierczynska and G. Lota, Carbon-Supported Manganese Dioxide as Electrode Material For Asymmetric Electrochemical Capacitors. *Chem Commun* **2014,** *9*, 2518-2534..

46. S. Chen, J. Zhu, X. Wu, Q. Han and X. Wang, Graphene Oxide-MnO_2 Nanocomposites for Supercapacitors. *ACS nano* **2010,** *4* (5), 2822-2830.

47. C. Liu, D. Gui and J. Liu, Preparation of MnO_2/graphene nanocomposite for the application of supercapacitor. *IEEE* **2014,** *177*, 177-182.

48. Thomas A. Mellan, Khomotso P. Maenetja, Phuti E. Ngoepe, Scott M. Woodley, C. Richard A. Catlow and Ricardo Grau-Crespo, Lithium and oxygen adsorption at the β-MnO_2 (110) surface. *J. Mater. Chem. A* **2013,** *1*, 14879-14887.

49. G.-R. Li, Z.-P. Feng, Y.-N. Ou, D. Wu, R. Fu and Y.-X. Tong, Mesoporous MnO_2/Carbon Aerogel Composites as Promising Electrode Materials for High-Performance Supercapacitors. *Langmuir* **2010,** *26* (4), 2209-2213.

50. Zhi, M.; Xiang, C.; Li, J.; Li, M.; Wu, N., Nanostructured carbon–metal oxide composite electrodes for supercapacitors: a review. *Nanoscale* **2013,** *5* (1), 72-88.

Chapter 2 Cotton-derived three-dimensional graphene current collector

2.1 Introduction

With the rapid increasing usage of electronic device, energy storage systems with high performance have been required. Among energy storage systems, supercapacitors have been developed as the rising energy storage device because of their high stability, superior power density, and quick charge-discharge processes[1-4]. Charges can be stored by the electrostatic force at the interface between the surface of active materials and electrolytes for supercapacitors, which are called EDLCs[5-7]. The active materials of EDLCs are mainly used by many carbon-based materials with large surface area. Among many carbon-based materials, graphene has been researched as a rising material for supercapacitor application[8-12]. With a mass production, graphene loses the outstanding electrical conductivity, which it causes low value of capacitance despite the large surface area[13]. In addition, the EDLCs have a limitation about the low value of energy density compared to batteries[14]. For the limitation, pseudo-capacitors have been introduced to achieve the higher capacitance than the EDLCs and high energy density like batteries[15-16]. Pseudo-capacitors are worked by utilizing both the electrostatic attractive forces and the redox reactions from the active electrodes of the transition metal oxides[17-21]. Transition metal oxides, known as RuO_2 and MnO_2, have advantages with high proton conductivity, high capacitance, and a wide potential window[22-26]. However, they suffer from poor conductivity and dead volume, which make it difficult to reach the theoretical capacitance as well as poor cycle stability[27].

Generally, three-dimensional metal-based current collectors like nanoporous gold (NPG) or nickel foam (NF) electrodes have been used because they provide fast electron and charge transport for high performance supercapacitors[28-30]. Due to an expensive cost and low surface area, they have trouble being commercialized even though they have unique properties. The large surface area is quite important factor as a current collector, which can increase active sites and decrease the dead volume of active electrodes[31]. For these reasons, three-dimensional metal current collectors have been studied. In particular, the fully connected three-dimensional metal is helpful for fast electron transportation due to the conductive networks[32]. It was also suggested that the resistance of welding metal nanowires presents lower about 2-10 times than non-treated nanowire by the Khang group[33]. However, NPG and NF electrode have a lower specific surface area because of their large density compare to carbon-based current collectors.

In this work, we present a facile and cost-effective method to fabricate nickel nanoparticle-coated

graphene foam (Ni-GF) as a three-dimensional current collector for supercapacitor. The entirely coated nickel nanoparticles on the surface of graphene foam play a role as a catalyst for the growth of graphene. They also help the graphene foam build the more conductive networks than before as a current collector. The Ni-GF showed large surface area, high electrical conductivity, and high-quality graphene. When nickel hydroxide ($Ni(OH)_2$) as an active material was performed to electrodeposition on the Ni-GF, it reached the outstanding capacitance and the high energy density. The $Ni(OH)_2$/Ni-GF nearly achieved the value of the theoretical capacitance with good kinetic properties for various electronic devices.

2.2 Experimental methods

2.2.1 Fabrication of Ni-GF, $Ni(OH)_2$/Ni-GF, and MnO_2/Ni-GF electrode

The commercial cotton was washed with acetone and coated by 2 M nickel chloride hexahydrate ($NiCl \cdot 6H_2O$) in water. The coated cotton was put into a vacuum desiccator for 12 hours. After fully dried, nickel chloride coated cotton was carbonized by the CVD process at 1000 ℃ for 2 hours with Ar and H_2 gas. The Ni-GF was prepared by slowly cooling after the heat treatment.

The $Ni(OH)_2$/Ni-GF electrode was fabricated by depositing nickel hydroxide ($Ni(OH)_2$) on the prepared Ni-GF. The Ni-GF electrode, Pt mesh, and Ag/AgCl(sat.) electrode worked as a working electrode, a counter electrode, and reference electrode. The electrodeposition of Ni(OH)2 was performed at -5 mA for 5 mins in a three-electrode system using 100mM nickel nitrate hexahydrate. Also, the MnO2/Ni-GF was prepared at 5 mA for 5 mins in 100 mM manganese acetate tetrahydrate via a similar method.

2.2.2 Chracterization

For the comparison of structures, the CC, NF, and Ni-GF were characterized by measuring FE-SEM (SEM, FEI/USA Nanonova 230) and TEM (FETEM, JEOL TEM 2100). The crystallinity of the electrodes was confirmed by X-ray diffraction measurement (XRD, Ragaku Co. high X-ray diffractometer D/MAZX 2500V/PC with Cu Kα radiation (λ = 1.5406 Å) with a scan rate of $1°s^{-1}$ in the 2θ range of 10°-80°). The form of bonding between the components of the electrodes was checked by Raman microscopy (Witec, alpha300R) and X-ray Photoelectron Spectroscopy (Thermo Fisher Scientific, ESCALAB 250XI). The determination of specific surface area, pore size, and pore volume were analyzed by the Brunauer-Emmett-Teller (BET) method with a Belsorp max system (Bel Japan).

2.2.3 Electrochemical tests

The electrochemical performance of the Ni-GF was determined both in a three-electrode system and in a two-electrode system using a system controlled electrochemical interface by computer (VMP3 biologic). In the case of a three-electrode system, the programs of cyclic voltammogram (CV) and galvanostatic charge-discharge (GCD) were tested by the Pt mesh as the counter electrode and Hg/HgO electrode as a reference electrode in 1 M KOH as the electrolyte. The $Ni(OH)_2$/Ni-GF electrode and the MnO2/Ni-GF electrode worked as the positive and the negative electrodes in a two-electrode system. Electrochemical impedance spectroscopy (EIS) was analyzed at a frequency range of 100 kHz-0.1 kHz by using a potentiostat (Versa STAT 3, AMETEK).

2.3 Results and discussion

A schematic diagram preparing the fabrication of Ni-GF with simple two-steps is provided in figure 2.1, according to the corresponding photographs. The washed commercial cotton was coated with 2 M nickel chloride solution and dried by a desiccator in a vacuum state. With removing hydroxyl groups, the drying process proposed that it is formed by the coordination of nickel ions in a dipping solution and oxygen ions in a cotton. The Ni-coated cotton was carbonized by the CVD process with argon and hydrogen gas. It provided the growth of graphene with the nickel particle as a catalyst, forming the entirely graphene on the surface of cotton. Figure 2.1 shows photographs of the commercial cotton, the dried nickel-coated cotton, and the Ni-GF with nearly retaining the similar sizes due to well-welded nickel particle in the cotton. The completed Ni-GF consists of nickel nanoparticles and graphene of the overall surface and has an enhanced electrical conductivity than a carbonized cotton.

The change morphologies of the carbonized cotton with no coating and the Ni-GF show the scanning electron microscope (SEM) images in Figure 2.2a-d. The Ni-GF can confirm the similar structure with the surface coated nickel nanoparticles, while the commercial cotton composed the form of many bundles of fiber connected each other. The Ni-GF also exhibit the decreased bundles of fiber compare to the commercial cotton because of the mass evaporation and reduction of nickel nanoparticles with the CVD process. The step is provided by a slight shrinkage and maintenance of three-dimensional structure. Figure 2.2d show the uniformly coated nickel nanoparticles, resulting in good electrical conductivity and fast charge transfer. Figure 2.2e-f exhibit the structure of the Ni-GF with coated nickel nanoparticles and graphene in the transmission electron microscopy (TEM) images. As shown in Figure 2.2f, it is confirmed by the nickel nanoparticles and the graphitic layers. The nickel nanoparticles of morphology were surrounded by the graphitic layers, causing enhanced efficiency of the electron transfer. Based on the CVD condition, we can develop the Ni-GF, resulting in the increased electrical conductivity and the effective electron/charge transfer.

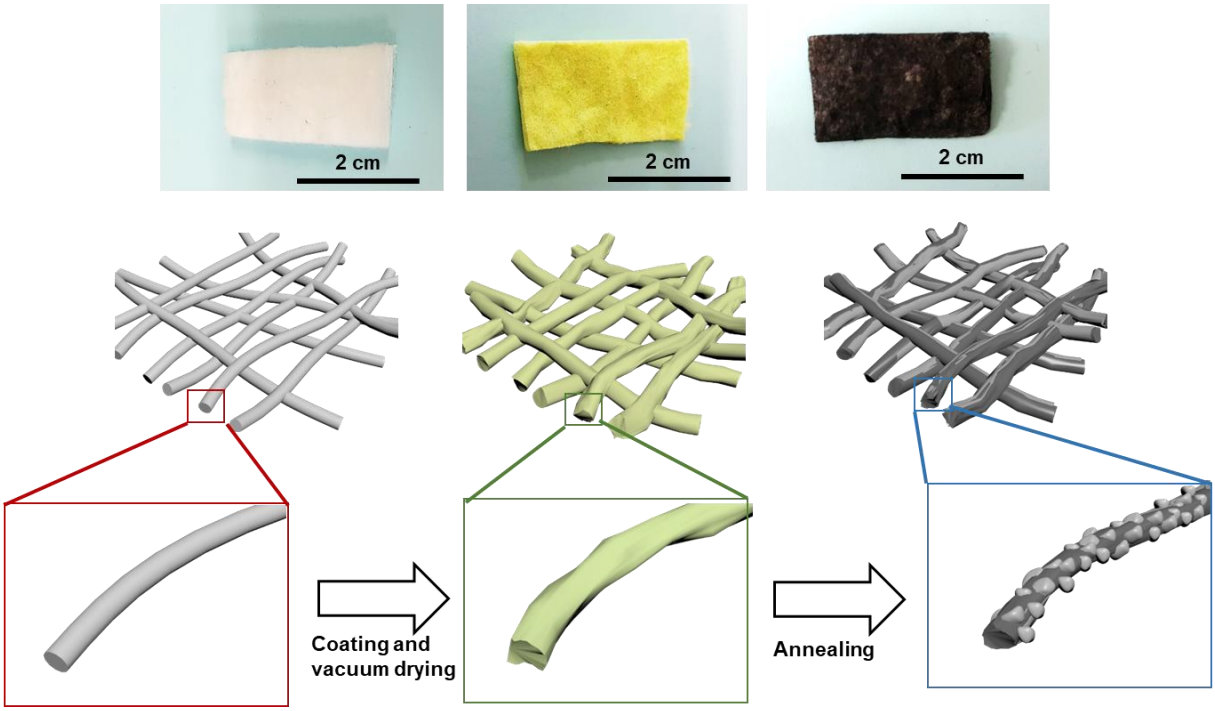

Figure 2. 1. Schematic illustration of the fabrication process for Ni-GF

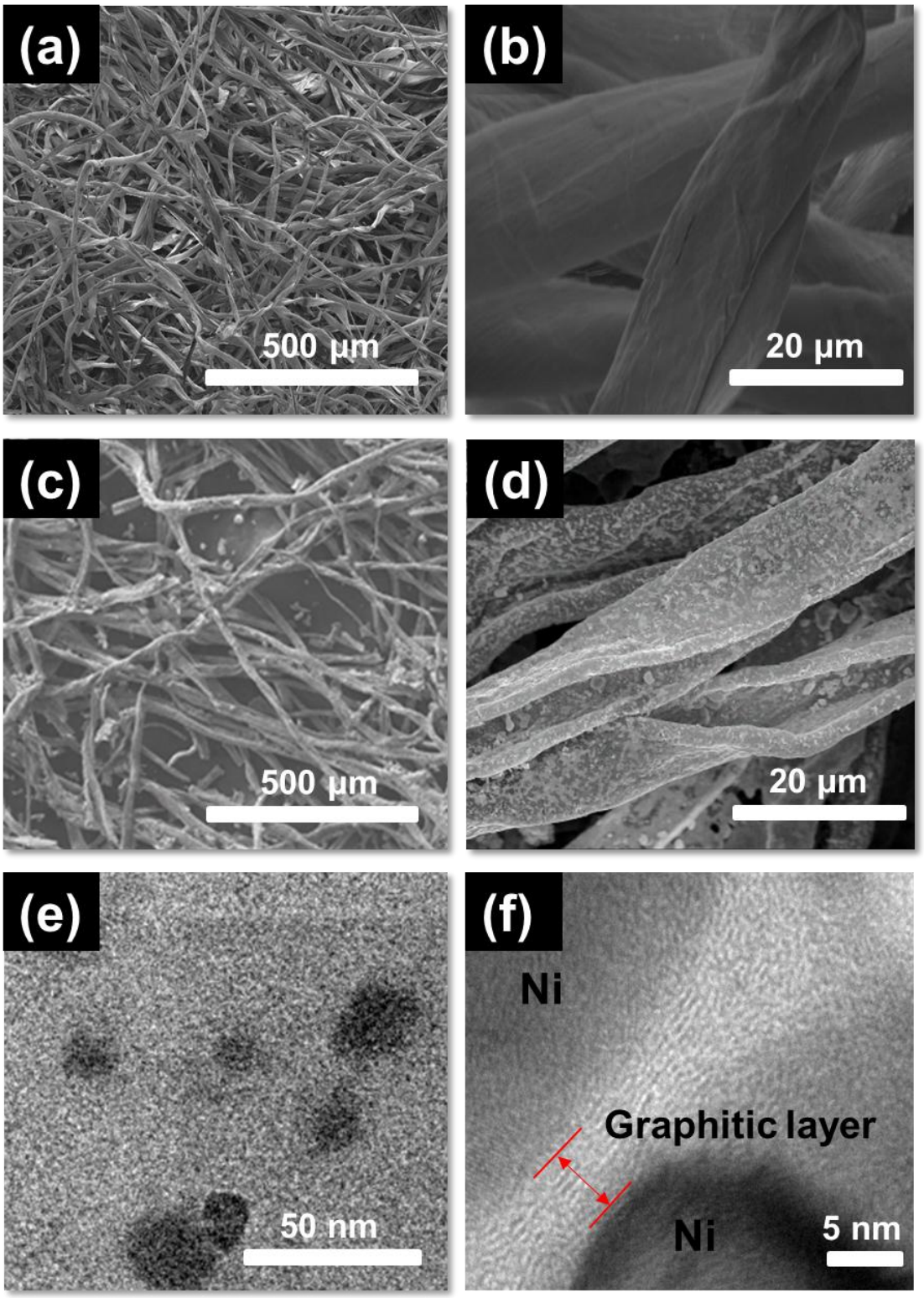

Figure 2. 2. SEM images: (a-b) the commercial cotton, (c-d) the Ni-GF and TEM images (e-f) of the

Ni-GF

As shown in Figure 2.3, the X-ray diffraction (XRD) patterns were checked after the CVD process. The XRD peaks could indicate the carbon and the nickel, confirming the Ni-GF. The domain of (002) plane of graphitic carbon can be identified by the peaks at 26.5^{o}, resulting in the growth of graphene, whereas the respectively strong peaks are explained as those of the reduction of Ni^{2+} by the CVD process with a hydrogen gas. The reduced nickel ions play a role as catalyst to create a graphene, corresponding to the plane of (111), (200), and (200) at 44.7^{o}, 52.0^{o}, and 76.4^{o}. This data can also demonstrate that nickel ions in the nickel chloride solution help the cotton form the graphene networks as catalyst, retaining the ion state without the oxidation process by the hydrogen gas.

The Raman spectroscopy (Raman) can check the existence of the graphene in Figure 2.4. There are the Raman peaks, corresponding to a D band, a G band, and a 2D band at 1350 cm^{-1}, 1580 cm^{-1}, and 2680 cm^{-1}. It can present the crystallinity according to the intensity ratio of the D band and the G band and the high quality compared to the intensity ration of the G band and the 2D band. The carbonized cotton with no coating process showed a low crystallinity with a ratio of I_D/I_G, whereas the Ni-GF with nickel particles showed the higher crystallinity than without nickel particles, achieving the ratio of I_D/I_G (0.57). The ratio of I_{2D}/I_G is determining the quality of graphene, reaching the few layers of graphene with a high ratio of I_{2D}/I_G (0.93) from the Ni-GF. These results can explain a high electrical conductivity and a large surface area, causing the Ni-GF to achieve the high performance for supercapacitors.

Further characterization of the Ni-GF was performed by X-ray photoelectron spectroscopy (XPS), shown in Figure 2.5. The $Ni2p_{1/2}$ and $Ni2p_{2/3}$ peaks at the binding energy of 869.9 eV and 852.6 eV detected in the Ni-GF, which confirmed the reduction of Ni^{2+} (Figure 2.5a). As appeared in Figure 2.5b, the C1s peak at the binding energy of 284.6 eV consists of regions both a sp^2-carbon at 284.5 eV and a sp^3-carbon at 284.9 eV, corresponding to the contents of 97% and 3%. The content of the sp^2-carbon is low in the C1s peak, indicating the high quality graphene according to the low defect sites.

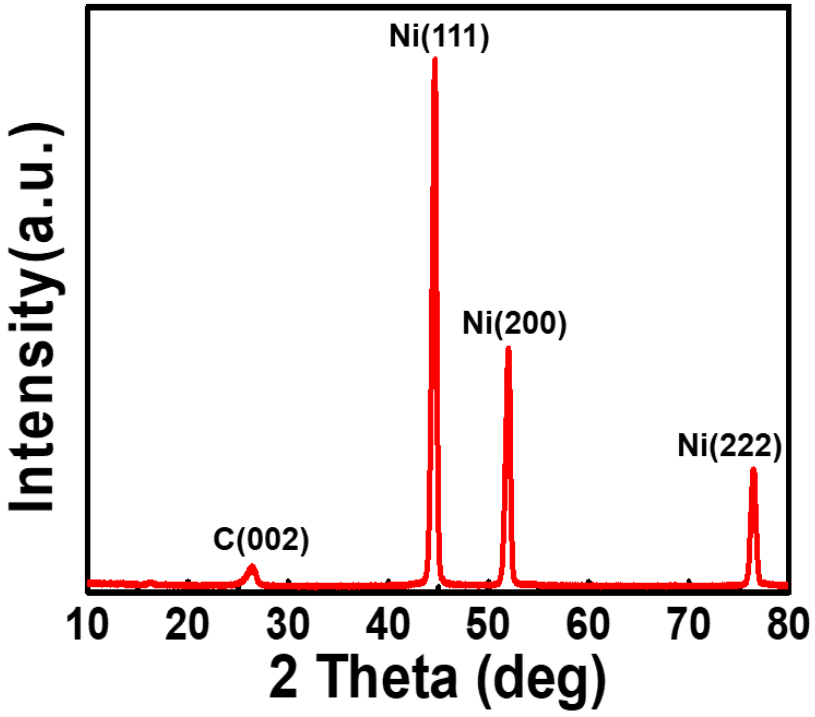

Figure 2. 3. XRD pattern of the Ni-GF.

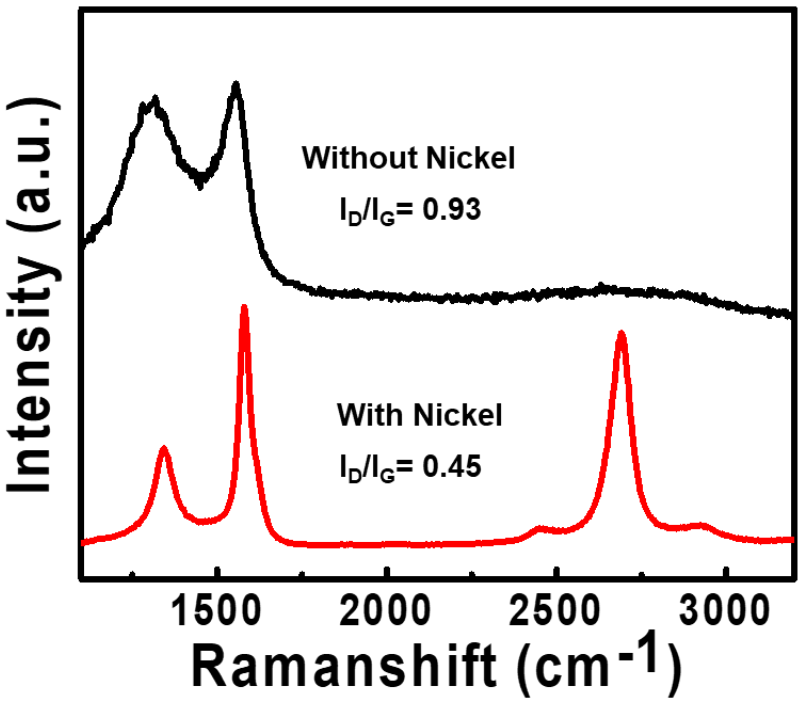

Figure 2. 4. Raman spectra compared to the carbonized cottons without nickel and with nickel.

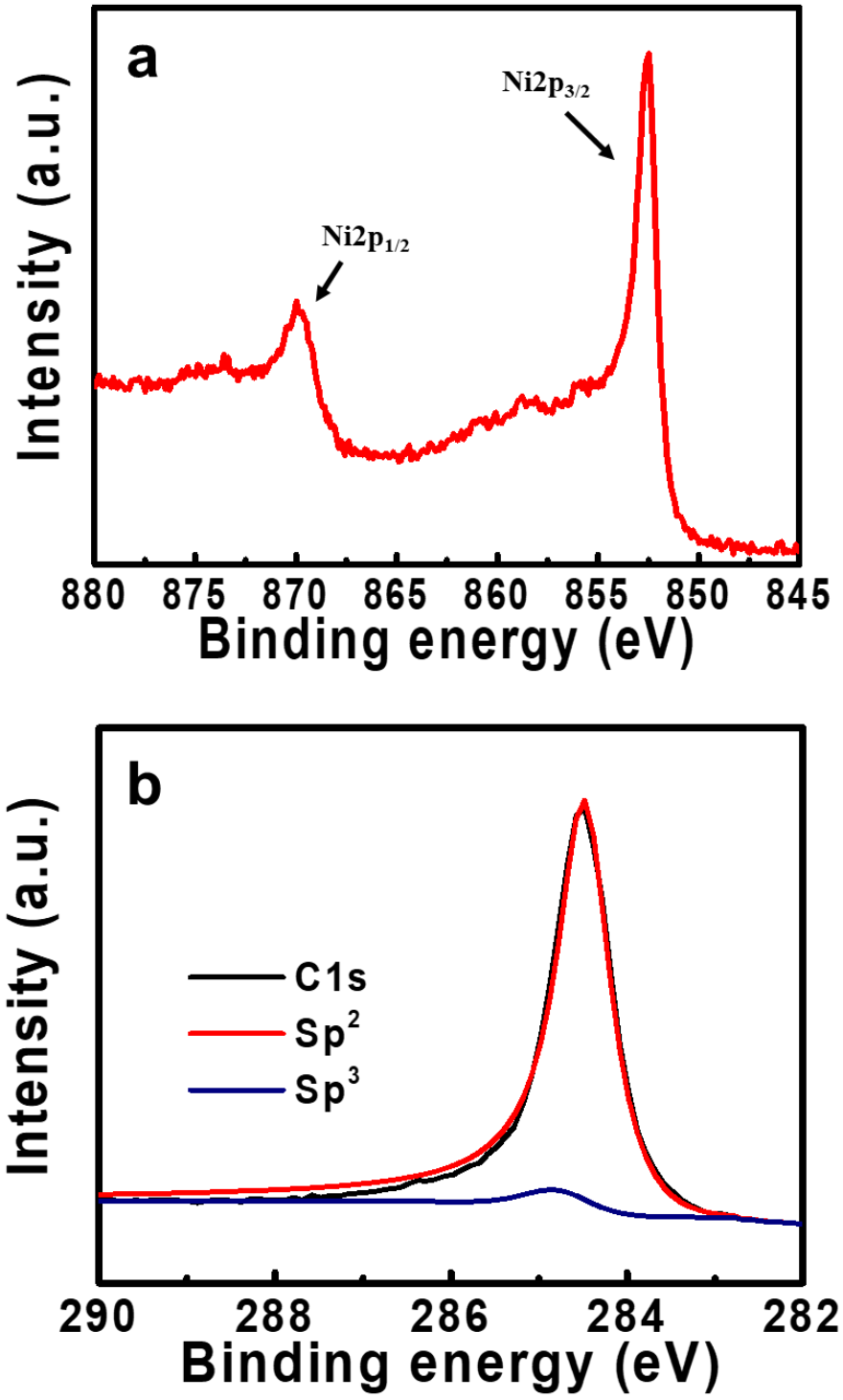

Figure 2. 5. XPS spectra of (a) $Ni2p_{1/2}$ and $Ni2p_{2/3}$ regions and (b) C1s region of the Ni-GF.

Specific surface area can be checked using a BET, including nitrogen adsorption/desorption isotherm curve and determination of pore size in Figure 2.6. As shown in Figure 2.6a, the shape of the

Ni-GF is near type IV according to a hysteresis loop, indicating that the structure consists of slight micropores and most mesopores[34]. The specific surface area of Ni-GF was 16.4 m^2g^{-1}, and the pore sizes are in the range of 1-30 nm due to the mass evaporation of nickel and carbon during the carbonization. Compared to commercial NF (0.1 m^2g^{-1}), the Ni-GF presented the high value of surface area, leading to improved electrolyte permeability and enhanced ion/electron pathways. The mesoporous Ni-GF is attributed to the fast ion transport in the electrolyte, resulting in the good performance for supercapacitor.

Figure 2.7 shows the XRD results of the Ni-GF before and after $Ni(OH)_2$ deposition. The XRD pattern in Figure 2.7b exhibits the peaks of the $Ni(OH)_2$ and the graphite oxide unlike the Ni-GF before electrodeposition. The words of green color can be confirmed to a α-$Ni(OH)_2$ (JCPDS, 38-0715) with the positions of peak at 13.5°, 33.7°, and 59.5°, corresponding to the (003), (006), and (110) planes[35]. The comparison of before and after electrodeposition is fairly indicated by the existence of $Ni(OH)_2$. The XRD data shows uniformly $Ni(OH)_2$-deposited Ni-GF electrode, which $Ni(OH)_2$ formed by the electrodeposition method plays a role as an active material.

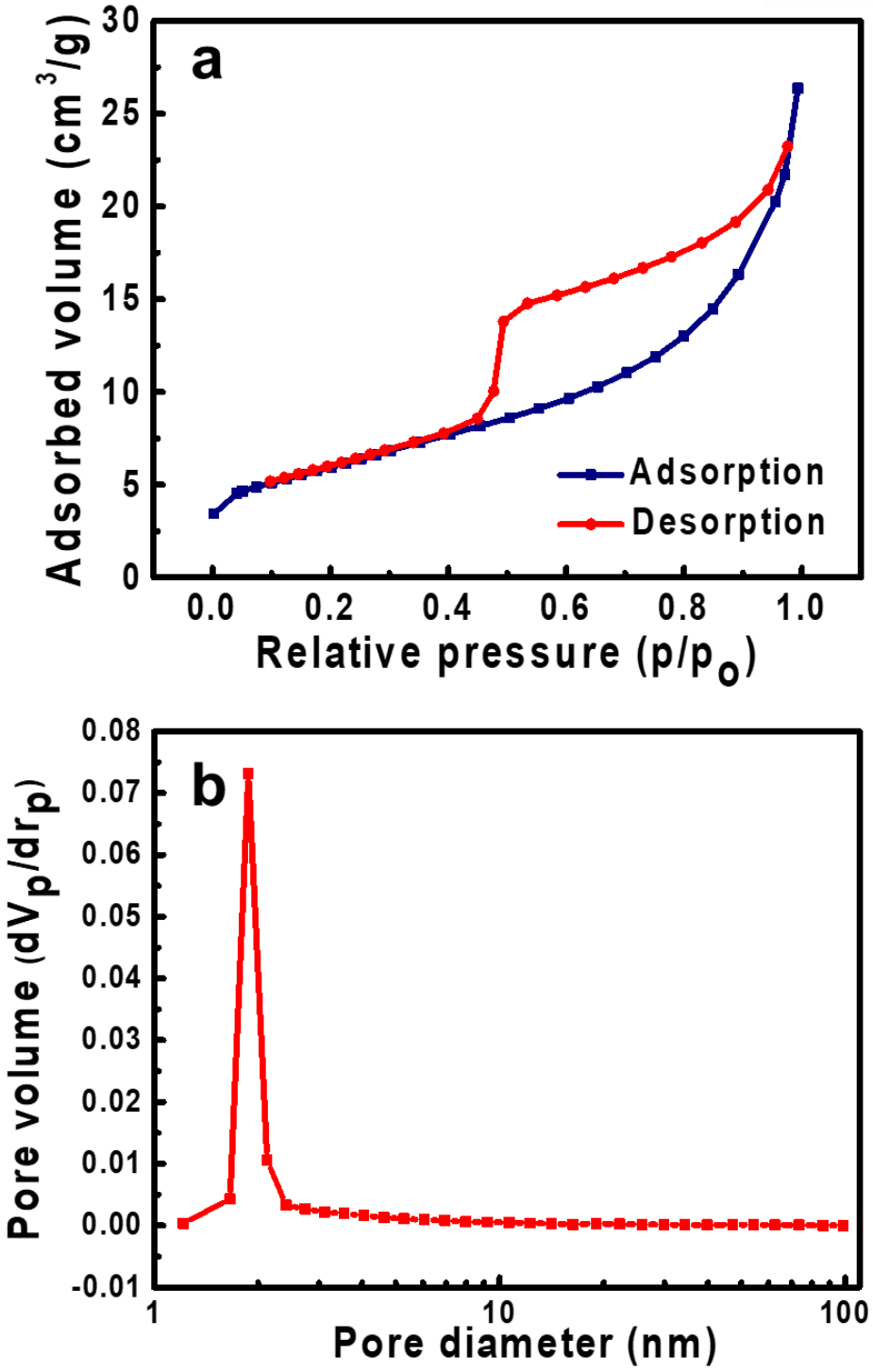

Figure 2. 6. BET analysis of (a) nitrogen adsorption isotherm curves and (b) determination of pore size of the Ni-GF.

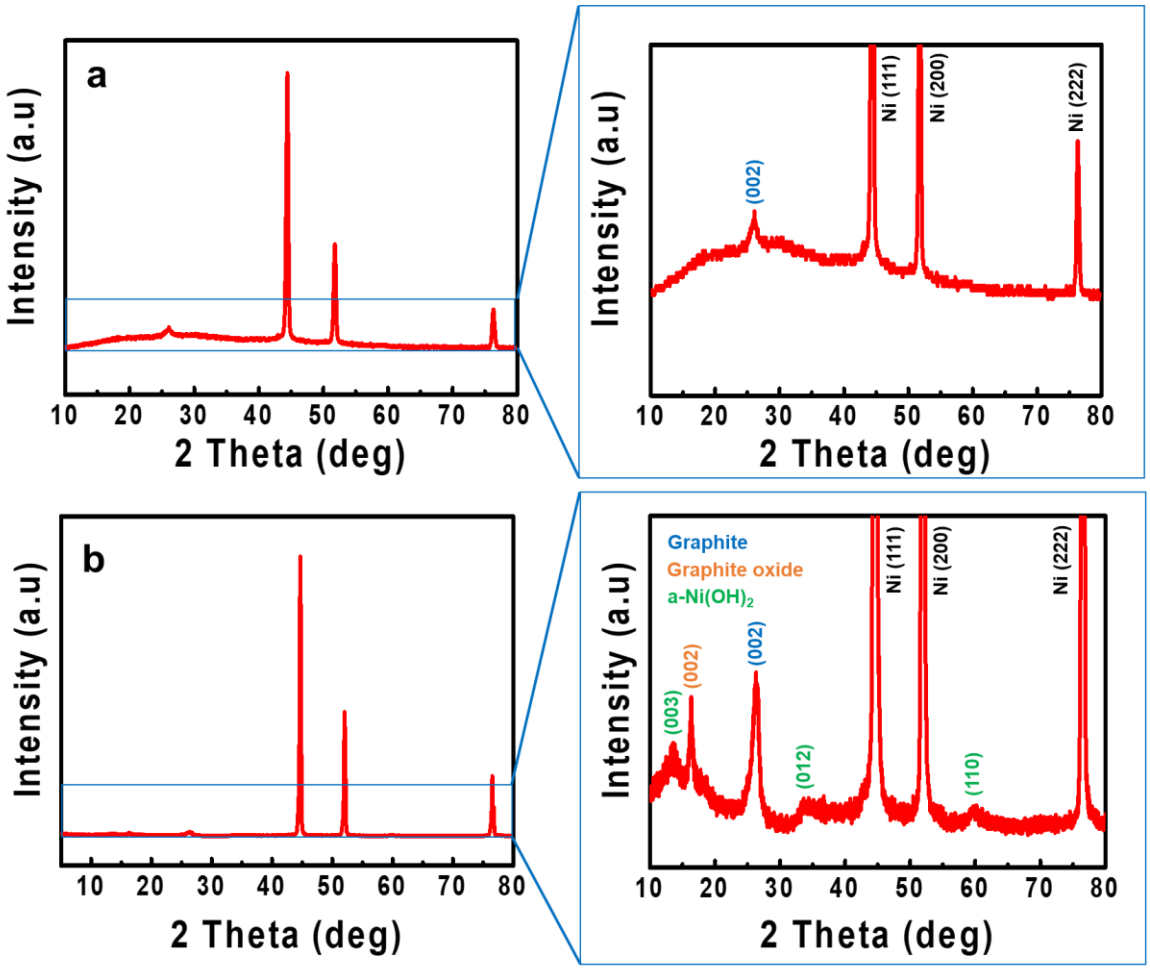

Figure 2. 7. TEM patterns of (a-b) the Ni-GF and (c-d) the $Ni(OH)_2$/Ni-GF.

Based on these characterizations of the Ni-GF, the supercapacitor performance is checked by the CV, GCD, and EIS tests. The CV test was performed at various scan rates to observe the shape of the CV curve. The shape of the CV curve shows the typical battery-like behavior with cathodic and anodic peaks, involved by the redox reaction between NiO and NiOOH (equation 2.1)[36].

$$NiO + OH^- \underset{\text{dischage}}{\overset{\text{charge}}{\rightleftharpoons}} NiOOH + e^- \quad (2.1)$$

As shown in figure 2.8, it is exhibited by electrochemical performances compared to the Ni-GF, NF, and carbonized cotton (CC). To compare their performances for supercapacitor, they were produced by electrodeposition of $Ni(OH)_2$ under the same condition as current collectors. The Ni-GF shows the largest area of the CV curve at 20 mV/s, indicating that the Ni-GF has the highest capacitance among them (Figure 2.8a). The capacitances were also calculated by GCD tests, resulting in the superior value of the Ni-GF compared to others. According to Figure 2.8a and b, the $Ni(OH)_2$/CC electrode has a poor electrical conductivity due to the capacitance obtained electrochemical tests. The CV curve of the Ni(OH)2/CC is showed, resulting in irreversible redox reaction. Except to the $Ni(OH)_2$/CC, the $Ni(OH)_2$/Ni-GF and the $Ni(OH)_2$/NF can check a reversible reaction in the CV curves (Figure 2.8a). However, the capacitance value of Ni(OH)2/Ni-GF is larger than the Ni(OH)2/NF because of the difference of the surface area. The Ni-GF has more active sites than NF, achieving the high performance for supercapacitor. The faster charge and ion transport of the Ni-GF is exhibited by the EIS analysis in more details. The Ni-GF and NF have smaller semicircles than the CC in the high range of frequency and a high value of slope in the low range of frequency, whereas the CC exhibits the largest semicircle and a small slope. Figure 2.8c means that the Ni-GF and NF have good ion diffusion properties. The Ni-GF is the best performance as a current collector due to the graphene with the porous structure even though NF has similar property with the Ni-GF.

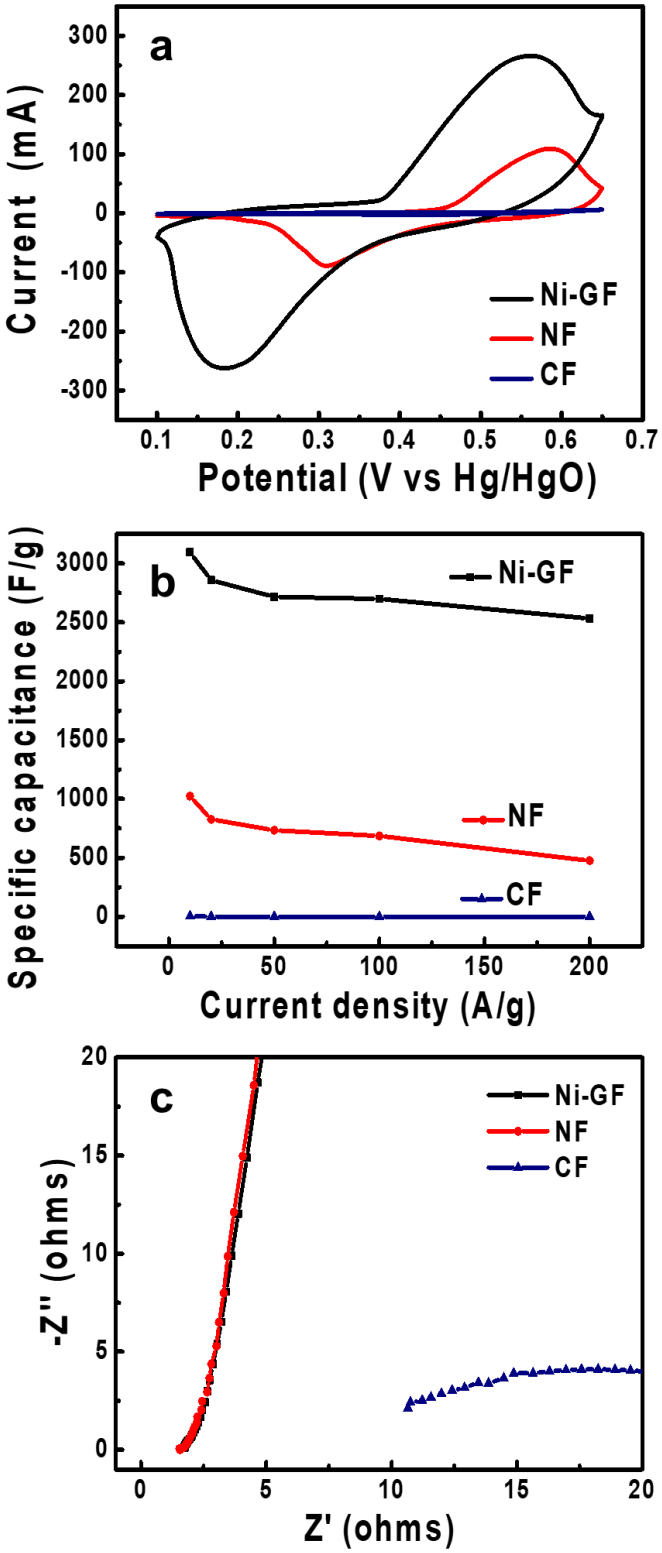

Figure 2. 8. Electrochemical behaviors of (a) CV curves at 20 mV s^{-1}, (b) GCD curves, and (c) Nyquist plots compared to the Ni-GF, NF, and CC.

The electrochemical behaviors of the $Ni(OH)_2$/Ni-GF electrode were determined in a three-electrode system as shown in Figure 2.9. Figure 2.9a provide the CV curves at scan rates of 1, 2, 5, 10, 20 mV s^{-1}, indicating that the area of the CV curves is increased according to increasing scan rate. The area of the overall curve at scan rates is related to the capacitance in the CV system (equation 2.2)[37].

$$C = \int_{V_a}^{V_b} I\, dV / mv(V_b - V_a) \quad (2.2)$$

The specific capacitance of the $Ni(OH)_2$/Ni-GF electrode is proved by a graph obtained by GCD curves based on equation 2.3 [38].

$$C = I\Delta t / m\Delta V \quad (2.3)$$

Figure 2.9b shows the GCD curves of the $Ni(OH)_2$/Ni-GF electrode, indicating that the Ni-GF has effective charge storage. The specific capacitance values were 3,214, 3,296, 3,099, 3,027, and 3,010 F g^{-1} at the current densities of 10, 20, 50, 100, and 200 A g^{-1}. The high capacitance is provided by the properties of the Ni-GF as a current collector, which have advantages of the high surface area and great electrical conductivity with the structures. The good cycle stability was confirmed for a three-electrode system in Figure 2.9c, retaining the capacitance after 10,000 cycles. These can be explained by the improved electrical conductivity and the large surface area of the Ni-GF, indicating the effective charge transport to the active material and the outstanding kinetics of the reversible redox reaction. Based on these results, it was used as a supercapacitor application.

It can be checked in Figure 2.10, indicating that the electrochemical properties are obtained by the $Ni(OH)_2$/Ni-GF//MnO_2/Ni-GF device in a two-electrode system for hybrid-capacitor. The CV curves of the device show oxidation and reduction of active materials, exhibiting the reaction for the MnO_2 in a low potential range and for $Ni(OH)_2$ in a high potential range with increased scan rate of 50 mV s^{-1} (Figure 2.10b). The capacitance of the asymmetric supercapacitor presented a good stability for 30,000 cycles. Figure 2.10a check the decrease for 5,000 cycles, whereas the high stability is above 60% for 30,000 cycles.

Further, the $Ni(OH)_2$/Ni-GF//MnO_2/Ni-GF device achieved the excellent energy density of 175 Wh kg^{-1} and power density 722 W kg^{-1} in a two-electrode system (Figure 2.10c). In comparison with other reported supercapacitors using $Ni(OH)_2$ as an active material, high value of energy density and power density is confirmed as shown in Table 2.1.

In our Ni-GF-based supercapacitor, the large surface area and the good kinetic property suggest improved electrical conductivity and high electrochemical performance with a simple fabrication method. Specially, the $Ni(OH)_2$/Ni-GF//MnO_2/Ni-GF hybrid-capacitor shows a superior value of energy density, resulting in new capacitor in the various fields.

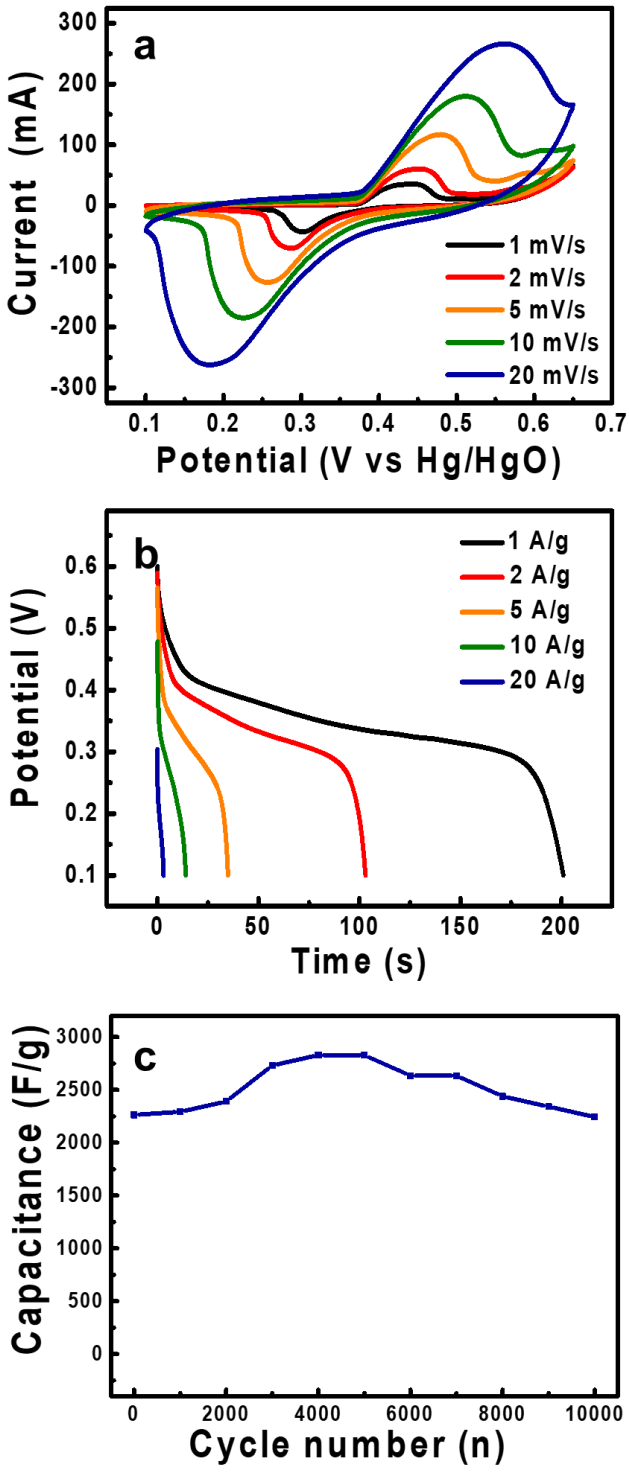

Figure 2. 9. Electrochemical behaviors of the $Ni(OH)_2$/Ni-GF electrode: (a) CV curves at different scan rates, (b) GCD curves at various current densities, (c) cycle stability until 10,000 cycles.

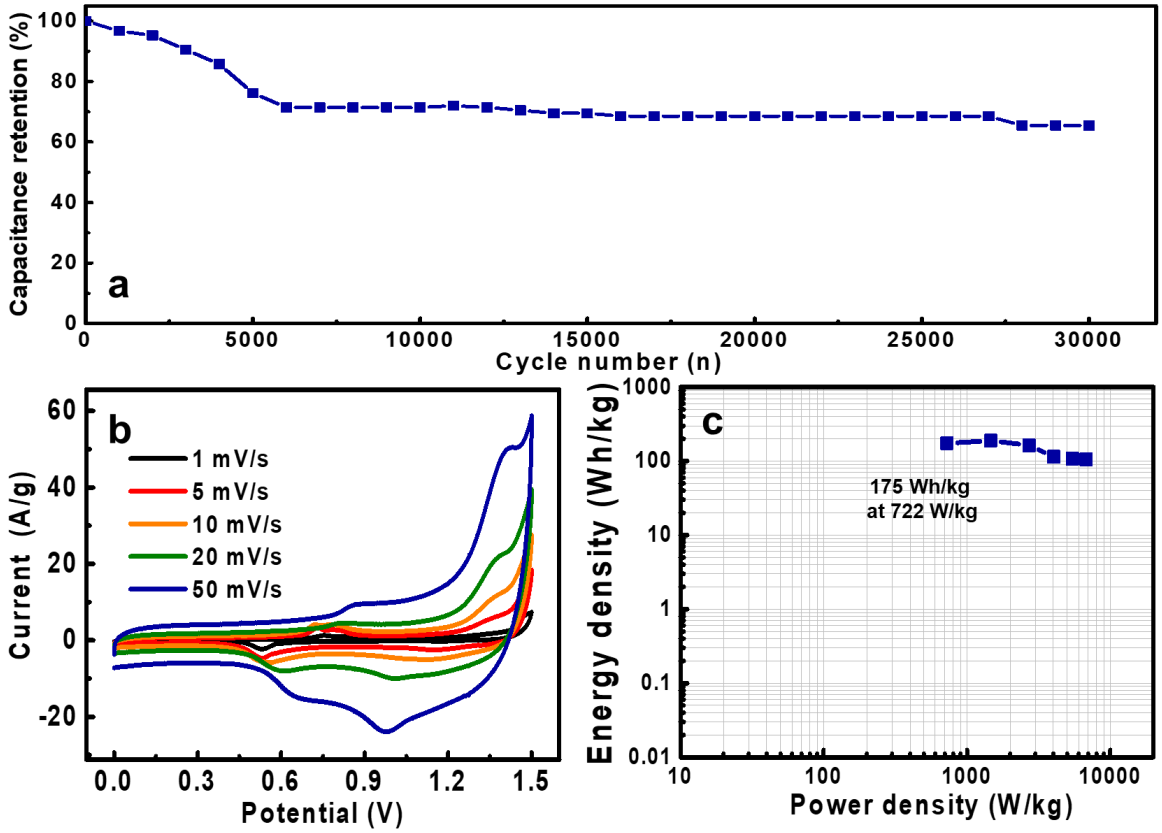

Figure 2. 10. Electrochemical performances of the hybrid-capacitor: (a) cycle stability for 30,000 cycles, (b) CV curves at different scan rates, (c) Ragone plot in a two-electrode system.

Table 2. 1. Comparison of previously reported $Ni(OH)_2$-based supercapacitors.

Materials	Energy density	Power density	Electrolyte
$Ni(OH)_2$/Ni-GF	175 Wh kg^{-1}	722 W kg^{-1}	1M KOH
$Ni(OH)_2$/RGO	75 Wh kg^{-1}	800 W kg^{-1}	2M KOH
$Ni(OH)_2$/graphene-porous graphene	77.8 Wh kg^{-1}	174.7 W kg^{-1}	6M KOH
$Ni(OH)_2$/MWCNT-PEDOT:PSS	58.5 Wh kg^{-1}	780 W kg^{-1}	1M KOH
$Ni(OH)_2$/pyrolytic graphite	98.3 Wh kg^{-1}	302 W kg^{-1}	1M NaOH
$Ni(OH)_2$/graphite	35.7 Wh kg^{-1}	490 W kg^{-1}	1M KOH

2.4 Conclusion

In conclusion, we have fabricated a new current collector that consists of high quality graphene and nickel composite (Ni-GF). The completed Ni-GF reveal more improved electrical conductivity than carbonized cotton and more enhanced surface area than commercial nickel foam. These properties result in achieving excellent capacitance and retaining high stability after 10,000 cycles in a three-electrode system. We also caused the Ni-GF fast electron transport and effective ion pathway in an electrolyte with the mesoporous structure. Furthermore, we developed an outstanding supercapacitor with the high value of capacitance and energy density using the $Ni(OH)_2$/Ni-GF//MnO_2/Ni-GF device.

2.5 References

1. Wang, G. P.; Zhang, L.; Zhang, J. J., A review of electrode materials for electrochemical supercapacitors. *Chem Soc Rev* **2012,** *41* (2), 797-828.
2. Simon, P.; Gogotsi, Y., Materials for electrochemical capacitors. *Nat Mater* **2008,** *7* (11), 845-854.
3. Zhi, M. J.; Xiang, C. C.; Li, J. T.; Li, M.; Wu, N. Q., Nanostructured carbon-metal oxide composite electrodes for supercapacitors: a review. *Nanoscale* **2013,** *5* (1), 72-88.
4. Huang, Y.; Liang, J. J.; Chen, Y. S., An Overview of the Applications of Graphene-Based Materials in Supercapacitors. *Small* **2012,** *8* (12), 1805-1834.
5. Zhu, Y. W.; Murali, S.; Stoller, M. D.; Ganesh, K. J.; Cai, W. W.; Ferreira, P. J.; Pirkle, A.; Wallace, R. M.; Cychosz, K. A.; Thommes, M.; Su, D.; Stach, E. A.; Ruoff, R. S., Carbon-Based Supercapacitors Produced by Activation of Graphene. *Science* **2011,** *332* (6037), 1537-1541.
6. Lee, J. S.; Kim, S. I.; Yoon, J. C.; Jang, J. H., Chemical Vapor Deposition of Mesoporous Graphene Nanoballs for Supercapacitor. *Acs Nano* **2013,** *7* (7), 6047-6055.
7. Yoon, J. C.; Lee, J. S.; Kim, S. I.; Kim, K. H.; Jang, J. H., Three-Dimensional Graphene Nano-Networks with High Quality and Mass Production Capability via Precursor-Assisted Chemical Vapor Deposition. *Sci Rep-Uk* **2013,** *3*.
8. Zhao, Y.; Li, X.; Yan, B.; Li, D.; Lawes, S.; Sun X., Significant impact of 2D graphene nanosheets on large volume change tin-based anodes in lithium-ion batteries: a review. *J. Power sources* **2015**, *274*, 869-884.
9. Yan, B.; Li, X.; Bai, Z.; Lin, L.; Chen, G.; Song, X.; Xiong, D.; Li, D.; Sun, X., Superior sodium storage of novel VO_2 nano-microspheres encapsulated into crumpled reduced graphene oxide. *J. Mater. Chem. A* **2017**, *5*, 4850-4860.
10. Yan, J.; Fan, Z.; Sun, W.; Ning, G.; Wei, T.; Zhang, Q.; Zhang, R.; Zhi, L.; Wei, F., Advanced asymmetric supercapacitors based on $Ni(OH)_2$/graphene and porous graphene electrodes with high energy density. *Adv. Funct. Mater.* **2012**, *22*, 2632-2641.
11. Liu, Y.; Wang, R.; Yan, X., Synergistic effect between ultra-small nickel hydroxide nanoparticles and reduced graphene oxide sheets for the application in high-performance asymmetric supercapacitor. *Sci. Rep.* **2015**, *5*, 11095.
12. Jiang, W.; Yu, D.; Zhang, Q.; Goh, K.; Wei, L.; Yong, Y.; Jiang, R.; Wei, J.; Chen, Y., Ternary hybrids of amorphous nickel hydroxide-carbon nanotube-conducting polymer for supercapacitors with high energy density, excellent rate capability, and long cycle life. *Adv. Funct. Mater.* **2015**, *25*, 1063-1073.
13. Lei, Z.; Christov, N.; Zhao, X., Intercalation of mesoporous carbon spheres between reduced graphene oxide sheets for preparing high-rate supercapacitor electrodes. *Energy Environ. Sci.* **2011**, *4*, 1866-1873.

14. Wu, Z.; Huang, X. L.; Wang, Z. L.; Xu, J. J.; Wang, H. G.; Zhang, X. B., Electrostatic Induced Stretch Growth of Homogeneous beta-Ni(OH)(2) on Graphene with Enhanced High-Rate Cycling for Supercapacitors. *Sci Rep-Uk* **2014,** *4*.

15. Conway, B. E.; Birss, V.; Wojtowicz, J., The role and utilization of pseudocapacitance for energy storage by supercapacitors. *J Power Sources* **1997,** *66* (1-2), 1-14.

16. Yu, L. T.; Jin, Y. Y.; Li, L. L.; Ma, J.; Wang, G. F.; Geng, B. Y.; Zhang, X. J., 3D porous gear-like copper oxide and their high electrochemical performance as supercapacitors. *Crystengcomm* **2013,** *15* (38), 7657-7662.

17. Lu, X. H.; Wang, G. M.; Zhai, T.; Yu, M. H.; Gan, J. Y.; Tong, Y. X.; Li, Y., Hydrogenated TiO2 Nanotube Arrays for Supercapacitors. *Nano Lett* **2012,** *12* (3), 1690-1696.

18. Cheng, C. W.; Fan, H. J., Branched nanowires: Synthesis and energy applications. *Nano Today* **2012,** *7* (4), 327-343.

19. Sugimoto, W.; Iwata, H.; Yasunaga, Y.; Murakami, Y.; Takasu, Y., Preparation of ruthenic acid nanosheets and utilization of its interlayer surface for electrochemical energy storage. *Angew Chem Int Edit* **2003,** *42* (34), 4092-4096.

20. Deng, M. J.; Song, C. Z.; Ho, P. J.; Wang, C. C.; Chen, J. M.; Lu, K. T., Three-dimensionally ordered macroporous Cu2O/Ni inverse opal electrodes for electrochemical supercapacitors. *Phys Chem Chem Phys* **2013,** *15* (20), 7479-7483.

21. Zhong, J. H.; Wang, A. L.; Li, G. R.; Wang, J. W.; Ou, Y. N.; Tong, Y. X., Co3O4/Ni(OH)(2) composite mesoporous nanosheet networks as a promising electrode for supercapacitor applications. *J Mater Chem* **2012,** *22* (12), 5656-5665.

22. Hu, C. C.; Chang, K. H.; Lin, M. C.; Wu, Y. T., Design and tailoring of the nanotubular arrayed architecture of hydrous RuO2 for next generation supercapacitors. *Nano Lett.* **2006,** *6* (12), 2690-2695.

23. Liu, T. C.; Pell, W. G.; Conway, B. E., Self-discharge and potential recovery phenomena at thermally and electrochemically prepared RuO2 supercapacitor electrodes. *Electrochim Acta* **1997,** *42* (23-24), 3541-3552.

24. Xia, H.; Meng, Y. S.; Yuan, G. L.; Cui, C.; Luc, L., A Symmetric RuO2/RuO2 Supercapacitor Operating at 1.6 V by Using a Neutral Aqueous Electrolyte. *Electrochem Solid St* **2012,** *15* (4), A60-A63.

25. Qu, Q. T.; Zhang, P.; Wang, B.; Chen, Y. H.; Tian, S.; Wu, Y. P.; Holze, R., Electrochemical Performance of MnO2 Nanorods in Neutral Aqueous Electrolytes as a Cathode for Asymmetric Supercapacitors. *J. Phys. Chem. C* **2009,** *113* (31), 14020-14027.

26. Kim, H.; Popov, B. N., Synthesis and characterization of MnO2-based mixed oxides as supercapacitors. *J Electrochem Soc* **2003,** *150* (3), D56-D62.

27. Ji, J.; Zhang, L. L.; Ji, H.; Li, Y.; Zhao, X.; Bai, X.; Fan, X.; Zhang, F.; Ruoff, R. S., Nanoporous $Ni(OH)_2$ thin film on 3D ultrathin-graphite foam for asymmetric supercapacitor. *ACS Nano* **2013**, *7*, 6237-6243.

28. Xing, W.; Qiao, S.; Wu, X.; Gao, X.; Zhou, J.; Zhuo, S.; Hartono, S. B.; Denisa, H.-J., Exaggerated capacitance using electrochemically active nickel foam as current collector in electrochemical measurement. *J. Power Sources* **2011**, *196*, 4123-4127.

29. Xiong, X.; Ding, D.; Chen, D.; Waller, G.; Bu, Y.; Wang, Z.; Liu, M., Three-dimensional ultrathin $Ni(OH)_2$ nanosheets grown on nickel foam for high-performance supercapacitors. *Nano Energy* **2015**, *11*, 154-161.

30. Kim, S.-I.; Kim, S.-W.; Jung, K.; Kim, J.-B.; Jang, J.-H., Ideal nanoporous gold based supercapacitors with theoretical capacitance and high energy/power density. *Nano Energy* **2016**, *24*, 17-24.

31. Wu, Z.-S.; Winter, A.; Chen, L.; Sun, Y.; Turchanin A.; Feng, X.; Mullen, K., Three-dimensional nitrogen and boron co-doped graphene for high-performance all-solid-state supercapacitors. *Adv. Mater.* **2012**, *24*, 5130-5135.

32. Yu, Z.; Tetard, L.; Zhai, L.; Thomas, J., Supercapacitor electrode materials: nanostructures from 0 to 3 dimensions. *Energy Environ. Sci.* **2015**, *8*, 702-730.

33. Yoon, S.-S.; Khang, D.-Y., Room-temperature chemical welding and sintering of metallic nanostructures by capillary condensation. *Nano Lett.* **2016**, *16* (6), 3550-3556.

34. Thommes, M., Physical adsorption characterization of nanoporous materials. *Chem. Ing. Tech.* **2010,** *82* (7), 1059-1073.

35. Min, J.; Liu, J.; Lei, M.; Wang, W.; Lu, Y.; Yang, L.; Yang, Q.; Liu, G.; Su, N., Self-assembly of parallelly aligned NiO hierarchical nanostructures with ultrathin nanosheet subunits for electrochemical supercapacitor applications. *ACS Appl. Mater. Interfaces* **2016**, *8* (1), 780-791.

36. Meher, S. K.; Justin, P.; Rao, G. R., Nanoscale morphology dependent pseudocapacitance of NiO: Influence of intercalating anions during synthesis. *Nanoscale* **2011**, *3* (2), 683-692.

37. Chen, W.; Fan, Z.; Gu, L.; Bao, X.; Wang, C., Enhanced capacitance of manganese oxide via confinement inside carbon nanotubes. *Chem. Commun.* **2010,** *46*, 3905-3907.

38. Kaempgen, M.; Chan, C. K.; Ma, J.; Cui, Y.; Gruner, G., Printable thin film suprcapacitors using single-walled carbon nanotubes. *Nano Lett.* **2009**, *3* (2), 683-692.

Chapter 3 Hybrid-capacitor material for the controlled ratio of metal colloid ions

3.1 Introduction

Nowadays, it shows that the rapid increase in the demand for portable and wearable electric devices and energy storage systems requires simple small scale but large-scale energy density and environmentally friendly device[1-2]. As one of the energy storage systems, supercapacitors have attracted great attention because of long-term cycle life, high power density value, and good operating safety at fast charge/discharge processes compared to batteries[3-6]. However, there is a main limitation of low energy density because of their energy storage mechanism, forming the electrical double layers on the surface of electrode[7-9]. In order to overcome the weakness, many researches have been reported using metal oxides as active materials for pseudo-capacitors. Pseudo-capacitors have two methods of storing energy: by using physically electrostatic forces in electrical double-layered capacitors (EDLCs) and using reversibly redox reactions in the surface of active materials[10-12]. It was widely used by pseudo-capacitors, indicating that the advantage was high capacitances according to a wide potential window. Although pseudo-capacitors provide good performances, they have a poor conductivity and low cycle stability[13-16]. For these reasons, hybrid-capacitors are on the rise as a promising energy storage system, combining the advantages with EDLCs and pseudo-capacitors. It can be challenged by achieving high specific capacitance or operating wide working voltage window. It has been to enhance the capacitance by utilizing many active materials such as transition metal oxides[17-18], and to widen the operating voltage range using organic electrolytes[19-20].

Among many types of active materials, transition metal oxides have been used to increase capacitance, which can be activated by redox chemistry in the electrode surface. However, the reversible redox reaction occurred only at the surface of active materials, indicating that the inner part in the active materials cannot act as a electrode[21-22]. In addition, the poor utilization leads to low capacitance and low energy density. Recently, the poor utilization problem was overcome by introducing the colloid system as a active material. For example, Xue group reported the new active materials based on inorganic salt like $CoCl_2$, demonstrating that the salt electrodes can show a fast and reversible redox reaction[23]. However, they explained the electrode materials as a pseudo-capacitor that is controversial problem at present. The colloid system was suggested the new charge storage mechanism by Liang et. al[24]. They achieved 353 Wh kg^{-1} of energy density at 2250 W kg^{-1} of power density, but the capacitance retained only 1.5% capacitance at 30 A g^{-1}. They showed that it was too much loss and poor stability although they reached high electrochemical performance.

In this study, by utilizing the colloid system in energy storage devices, I challenged a hybrid-capacitor with the ratio of Ni^{2+} and Co^{2+} (1:1) electrode as a active material and carbonized cotton as a current collector. The Ni^{2+} and Co^{2+} colloidal electrode (NC) was utilized by redox reactions in whole colloids unlike transition metal oxides for pseudo-capacitor. In addition, the carbonized cotton (CC) plays a role of a current collector to help the enhancement of stability from the colloid electrode. The NC/CC electrode has improved capacitance and better stability than before reports. A device consisting of the NC/CC cathode and Mn^{4+}-colloidal anode (Mn/CC) shows good rate capability and enhanced energy density.

3.2 Experimental methods

3.2.1 Fabrication of carbonized cotton

The commercial cotton was washed with acetone and dried at 60 ℃ for 12 hours. After fully dried, washed cotton was carbonized by the CVD process at 1000 ℃ for 1 hours with argon gas. The CC was fabricated by slowly cooling after annealing.

3.2.2 Preparation of colloidal electrodes in a three-electrode system

For the comparison of behaviors in a three-electrode system, nickel chloride hexahydrate salts, carbon black, and polyvinylidene fluorine were mixed with the ratio of 6:3:1. The resulting slurry was pated onto a graphite current collector and dried at 60 ℃ for 3 hours. The Co^{2+} and Ni^{2+}:Co^{2+} (1:1)-colloidal electrode were prepared following same process like a Ni^{2+}-colloidal electrode.

3.2.3 Production of NC/CC and Mn/CC electrodes for hybrid-capacitor

The NC/CC electrode was fabricated by dip-coating 1 mmol nickel chloride hexahydrate in ethanol on the prepared CC and then dried naturally. The Mn/CC was also prepared by a similar method. The NC/CC//Mn/CC device was combined with the NC/CC and the Mn/CC as positive and negative electrode, respectively. The filter paper separates the two electrodes and electrolyte is used by 1M KOH. The prepared device was performed to in situ activation of colloidal electrodes by the cyclic voltammetry system. The device was completed after 20 cycles, forming activated colloidal electrodes.

3.2.4 Characterization

For the structures and the detection of elements with materials, the CC, NC/CC, and Mn/CC were characterized by using FE-SEM (SEM, FEI/USA Nanonova 230). The bonding of the CC after carbonization was checked by Raman microscopy (Witec, alpha300R).

3.2.5 Electrochemical tests

The electrochemical performance was evaluated using cyclic voltammetry (CV) and galvanostatic charge-discharge (GCD) by a computer controlled electrochemical interface (VMP3 biologic). The Ni^{2+}, Co^{2+}, and Ni^{2+}:Co^{2+} (1:1)-colloidal electrodes were performed with the Pt mesh a Hg/HgO electrode as the counter electrode and reference electrode in 1 M KOH as the electrolyte. The NC/CC//Mn/CC device was measured in a two-electrode system. Electrochemical impedance spectroscopy (EIS) was analyzed at a frequency range from 100 kHz to 0.1 kHz by using a potentiostat (Versa STAT 3, AMETEK).

3.3 Results and discussion

Figure 3.1 presents the overall fabrication process of the NC/CC electrode. First, a commercial cotton was washed in acetone and dried at 60 ℃ for 12 hours. Then, the dried cotton was reacted to heat treatment by the CVD process at 1000 ℃ for 1 hour with argon atmosphere. With obtaining many oxygen groups, the carbonized cotton (CC) was reacted by O_2 plasma. The treated CC was coated with 1 mmol nickel chloride solution and 1 mmol cobalt chloride solution in ethanol, and dried at temperature of 25 ℃. The oxygen group in the CC played a role of connecting metal colloid ion, forming the uniformly coated Ni^{2+} and Co^{2+} colloid ions on the CC. In addition, the electrode including Mn2+ colloid ion was fabricated by the following method in Figure 2.1. After preparing the all electrodes, it was performed to the in situ electrochemical activation by the cyclic voltammetry test. For example, the following activation process occurred by the strong bonding between Ni^{2+} and OH^- in the case of $NiCl_2$-coated electrode (equation 2.1)[25].

$$NiCl_2 + OH^- \rightarrow Ni(OH)Cl + Cl^- \rightarrow Ni(OH)_2 + Cl^- \quad (2.1)$$

In addition, the Co^{2+} and Mn^{2+} colloidal electrodes were showed with similar reactions (equation 2.2. and 2.3)[26-27].

$$CoCl_2 + OH^- \rightarrow Co(OH)Cl + Cl^- \rightarrow Co(OH)_2 + Cl^- \quad (2.2)$$

$$MnCl_2 + OH^- \rightarrow Mn(OH)Cl + Cl^- \rightarrow Mn(OH)_2 + Cl^- \quad (2.3)$$

The structure of colloidal electrodes was confirmed as shown in Figure 3.2 and 3.3. The fibers composed many carbon sources, including the CC. In addition, the images revealed that the nickel and cobalt ions are uniformly coated on the surface of CC as well as manganese ions using an energy dispersive spectrometer (EDS).

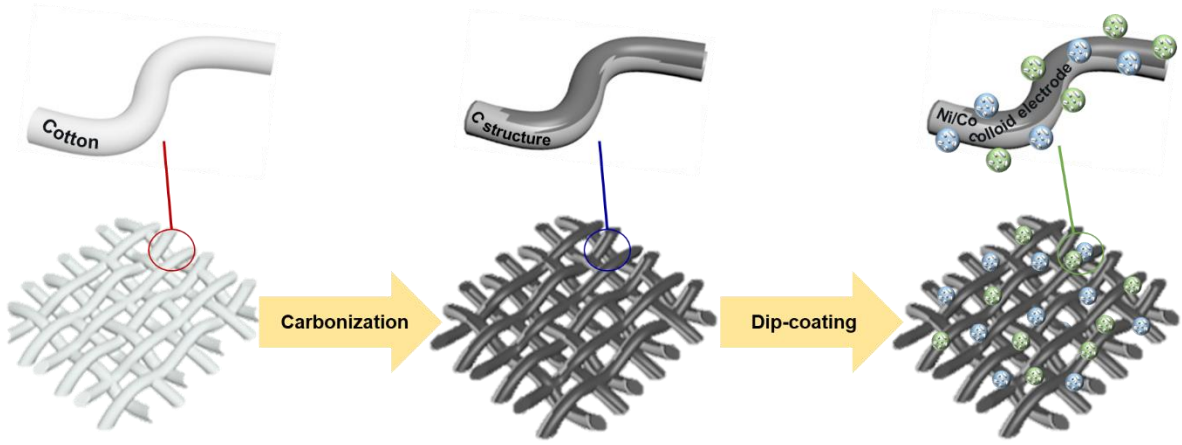

Figure 3. 1. Schematic diagram showing the fabrication process of the NC/CC.

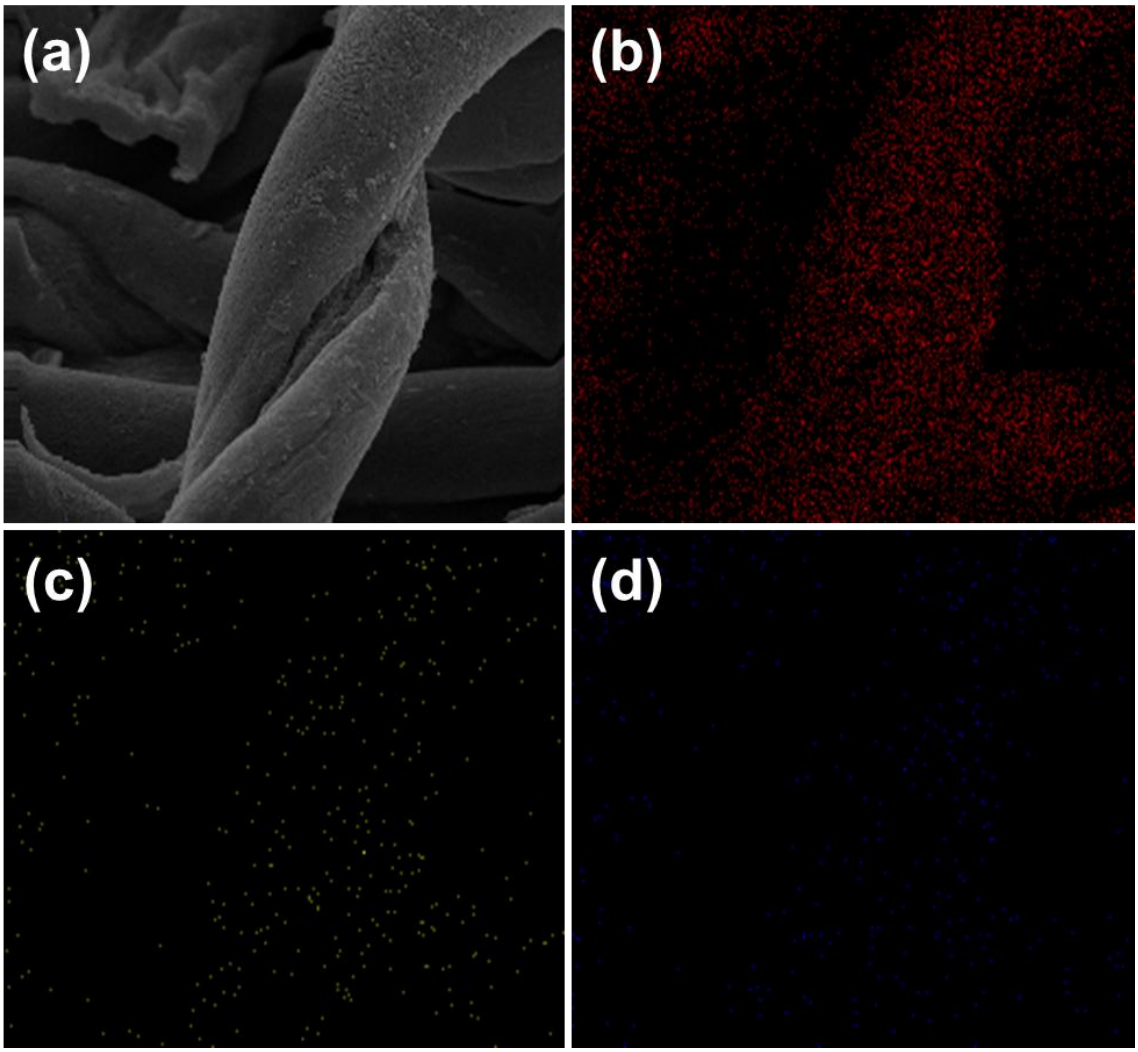

Figure 3. 2. (a) SEM images of the NC/CC and elements mapping of the NC/CC: (b) carbon (in red), (c) nickel (in yellow), and (d) cobalt (in blue)

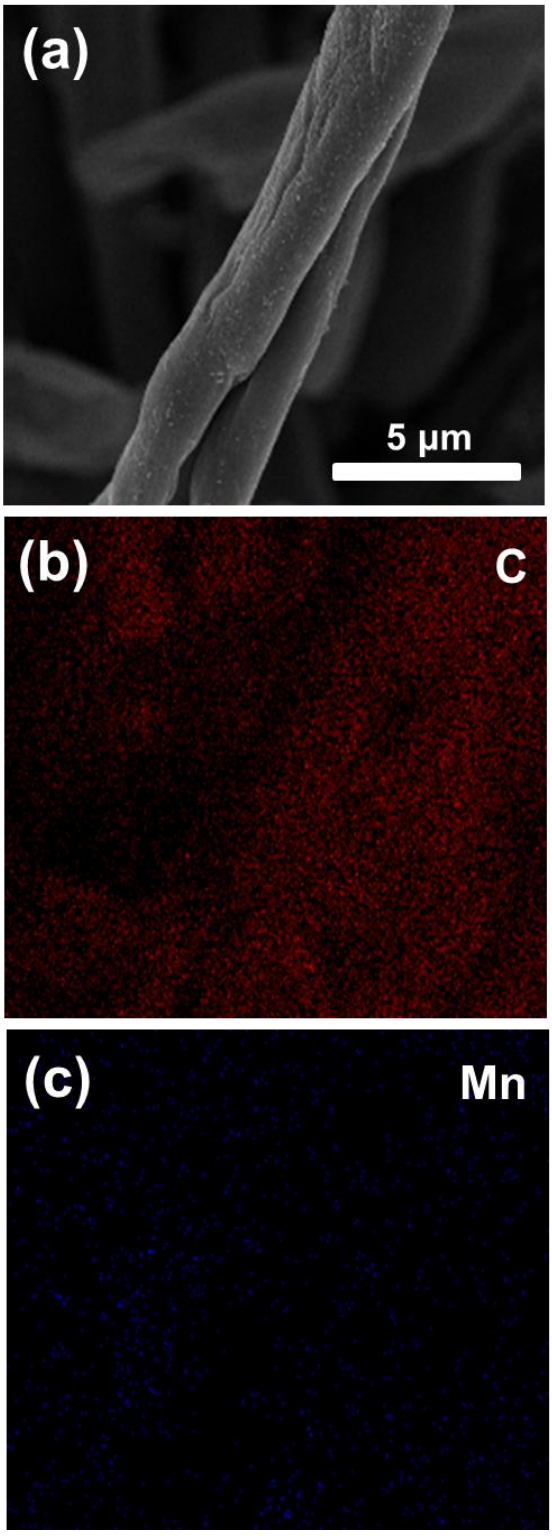

Figure 3. 3. (a) SEM images of the Mn/CC and elements mapping of the NC/CC: (b) carbon (in red), (c) manganese (in blue).

The electrodes consisting of Ni^{2+} and Co^{2+}, were performed to in situ activation using a cyclic voltammetry program. The ions in the colloidal electrode exchanged each other during the activation process. First, Cl^- ions in the $NiCl_2$ exchanged OH^- ions in the electrolyte of KOH when Ni^{2+}-colloid electrode reacted with CV cycling, forming $Ni(OH)_2$ in the substrate electrode. Co^{2+}-colloid electrode was also activated by the similar process such as the reaction of Ni-electrode. The result of activation process was to form the $Ni(OH)_2$ and $Co(OH)_2$ in the electrode.

After the activation process, the $Ni(OH)_2$ formed in the case of Ni^{2+}-colloid electrode and $Co(OH)_2$ formed in the case of Co^{2+}-colloid electrode reacted with KOH electrolyte in a three-electrode system (Figure 3.5). Figure 3.5a showed the reversible faradaic redox reactions as follows[28]:

$$Ni(OH)_2 + OH^- \Leftrightarrow NiOOH + H_2O + e- \quad (2.4)$$

The anodic peak at 0.47 V and cathodic peak at 0.34 V with the scan rate of 1 mV s^{-1} in the CV curves were presented with the oxidation and reduction processes of the nickel ions ($Ni^{3+} \Leftrightarrow Ni^{2+}$). In addition, a pair of redox peaks is showed to redox reaction for the Co2+-colloid electrode, indicating that the following reversible reactions occurred in Figure 3.4c[29].

$$Co_3O_4 + OH^- + H_2O \Leftrightarrow 3CoOOH + H_2O + e^- \quad (2.5)$$

The Co_3O_4 was formed by $Co(OH)_2$ according to the in situ activation. Figure 3.4c indicated that it was confirmed by the anodic and cathodic peaks similarly to redox reaction of nickel ions. The shape of CV curves was non-rectangular, corresponding to the battery-like faradaic redox reaction. The characteristics of nickel and cobalt emerged in Figure 3.4. In the case of $Ni(OH)_2$, it has various properties such as the theoretical capacitance of 2,584 F g^{-1} and the poor conductivity, causing the low stability[30]. However, the $Co(OH)_2$ has the higher theoretical capacitance of 3,560 F g^{-1} as well as the better stability than the $Ni(OH)_2$[31].

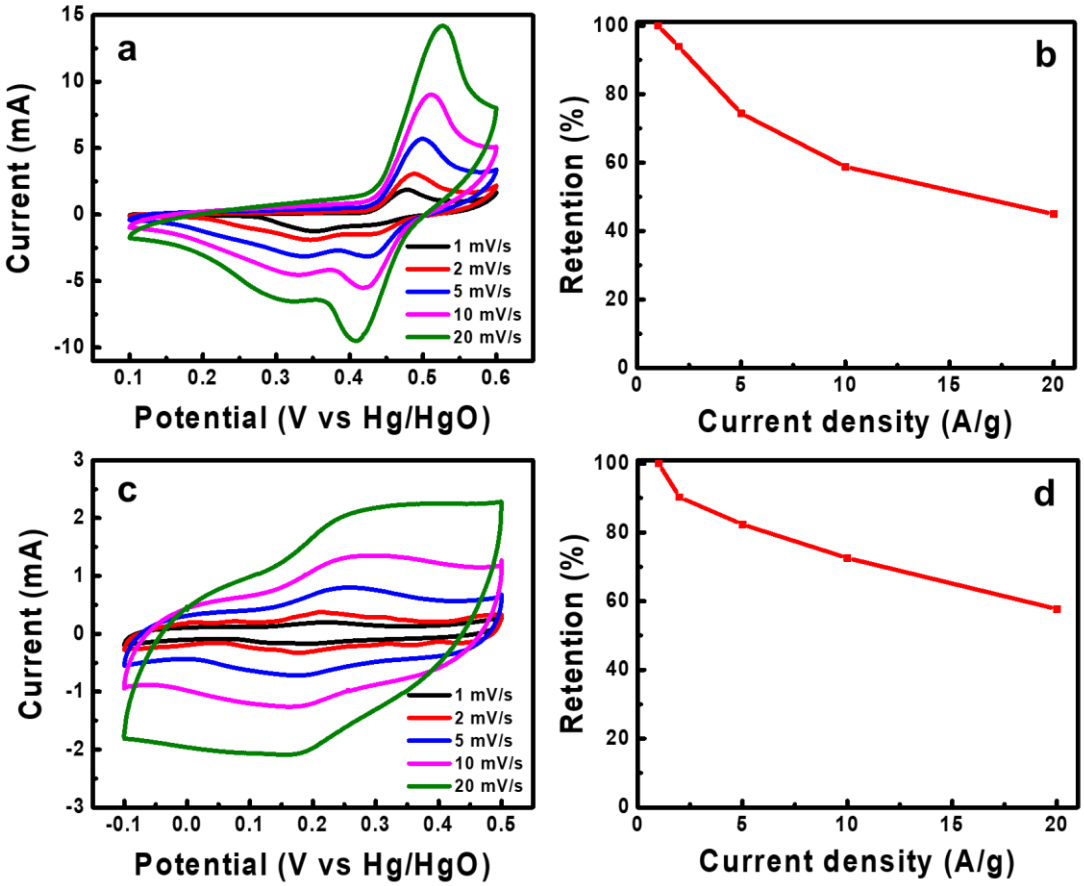

Figure 3. 4. Electrochemical behavior of (a-b) Ni^{2+}-colloid electrode and (c-d) Co^{2+}-colloid electrode in a three-electrode system.

Figure 3.5 showed the comparison of the various ratio with Ni^{2+} and Co^{2+}, corresponding to 1:1, 2:1, and 1:2. The Ni^{2+}:Co^{2+} (1:1)-colloid electrode revealed higher stability than the Ni^{2+}-colloid electrode as well as better performance than the Co^{2+}-colloid electrode, whereas the ratio of 2:1 presented with poorer stability than previous electrode. In addition, the high stability is showed with high current density for Ni^{2+}:Co^{2+} (1:2)-colloid electrode. Electrochemical properties such as stability and performance were determined by the contents with ratio of Ni^{2+}:Co^{2+}, as shown in Figure 3.5. The Ni^{2+}:Co^{2+} (2:1)-colloid electrode achieved the capacitance value of 450 F g^{-1} at a current density of 1 A g^{-1}. However, the capacitance value of 401 F g^{-1} was showed at same current density for the Ni^{2+}:Co^{2+} (1:1)-colloid electrode with a same condition of mass loading. It has better stability at high current density even though the Ni^{2+}:Co^{2+} (2:1)-colloid electrode has higher performance than it, because of the increased contents of cobalt ions. In addition, there is similar but distinct difference in comparison between the ratio of 1:1 and 1:2. With same mass loading, there is big difference of the capacitances that is 388 F g^{-1} for 1:1 and 339 F g^{-1} for 1:2. However, they showed a similar tendency in terms of stability with high current density (Figure 3.5b and f). It proved that stability was well-retained when the electrode consisting of nickel hydroxide is combining the slight cobalt hydroxide.

Mn^{2+}-colloid electrode also presented the electrochemical behavior in a three-electrode system, as shown in Figure 3.6. Therefore, the Mn^{2+}-colloid electrode played a role of a negative electrode and the Ni^{2+}:Co^{2+} (1:1)-colloid electrode also played a role of a positive electrode, indicating that two electrodes was formed to hybrid capacitor.

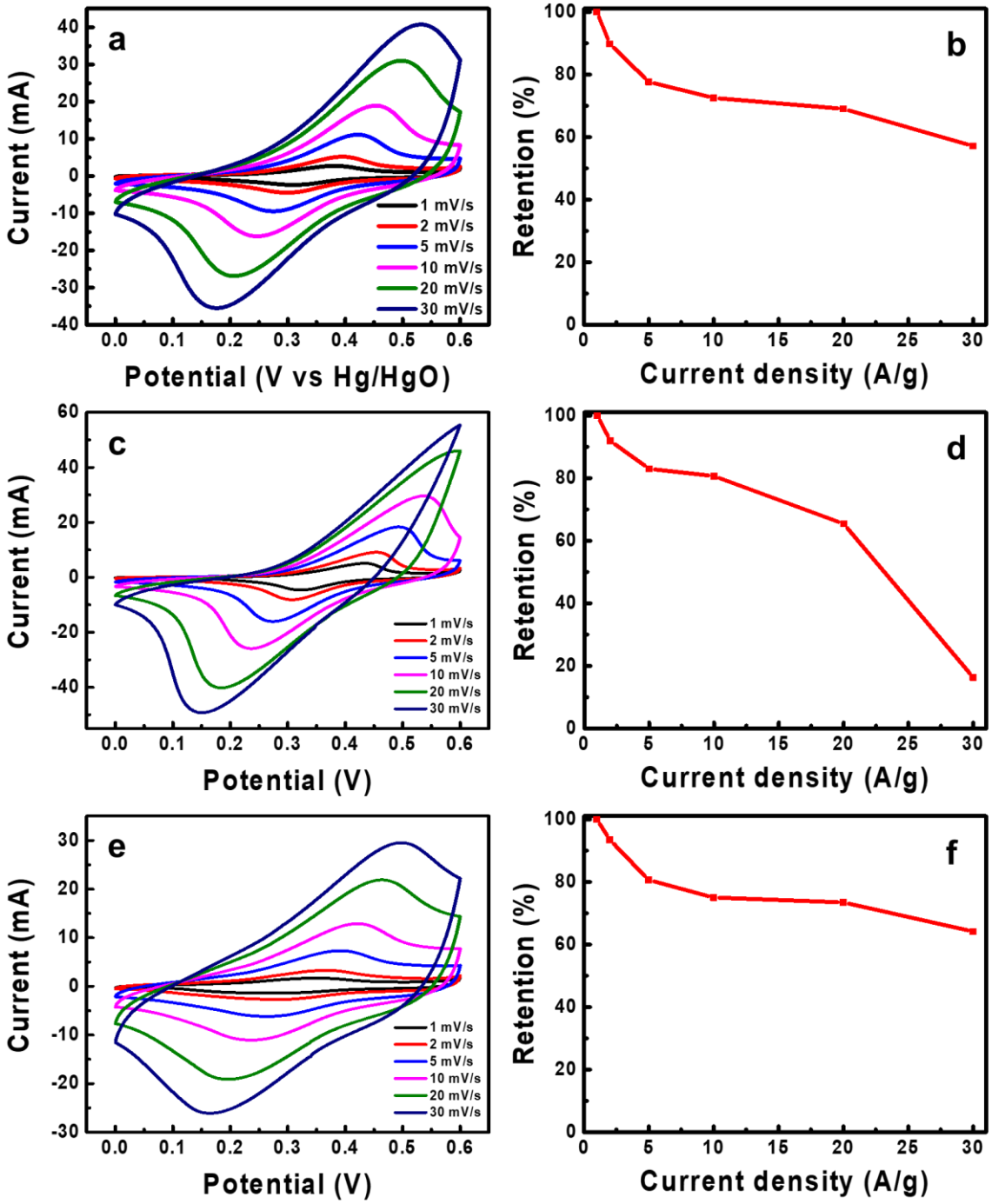

Figure 3. 5. Electrochemical behaviors in comparison of (a-b) Ni^{2+}:Co^{2+} (1:1)-colloid electrode, (c-d) Ni^{2+}:Co^{2+} (2:1)-colloid electrode, and (e-f) Ni^{2+}:Co^{2+} (1:2)-colloid electrode in a three-electrode system.

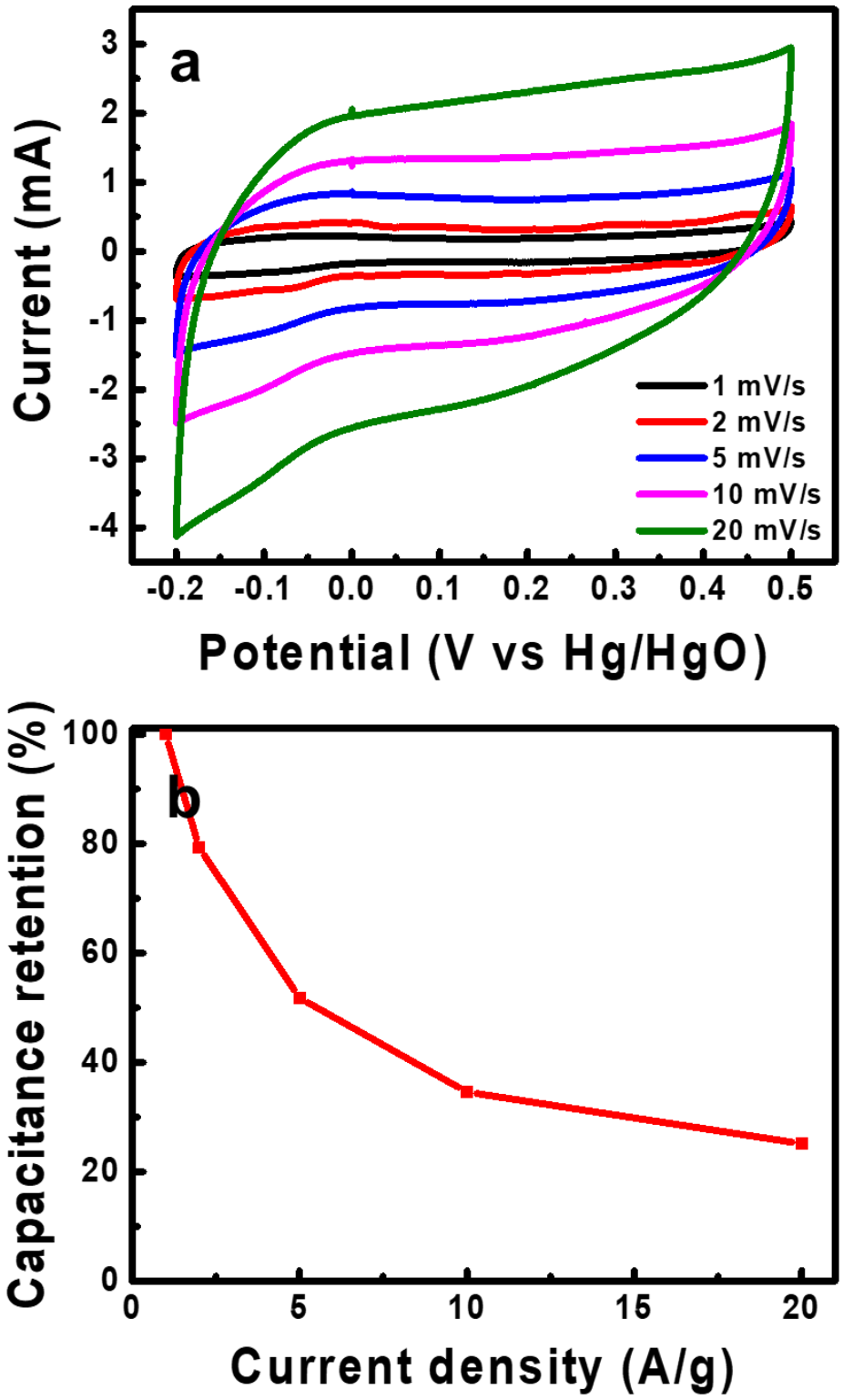

Figure 3. 6. Electrochemical performance of (a-b) Mn^{2+}-colloid electrode in a three-electrode system.

The prepared colloid electrodes were assembled with a hybrid capacitor device in order to measure electrochemical performance as a charge storage. The carbonized cotton was used to overcome the poor cycle stability and to support the colloid electrodes. Coin cell consisting of the Ni^{2+}:Co^{2+} (1:1) and Mn^{2+}-colloid electrode in the CC (1 cm X 1 cm) was fabricated and tested. Figure 3.7a showed the wide potential window range, combining the Ni^{2+}:Co^{2+} (1:1) and Mn^{2+}-colloid electrode. As shown in Figure 3.7b, the device exhibited areal capacitances of 65, 51, 35, 28, 17, and 17 mF cm^{-2} at various current densities of 1, 2, 5, 10, 20, and 30 mA cm^{-2}, respectively. With high current density, the stability was retained until 27 %, compared to the stability of 0% using a graphite as a current collector (Figure 3.8). The carbonized cotton has oxygen groups after treated using O_2 plasma, indicating that the nickel, cobalt, and manganese ions were performed to coordinate covalent bonds between the oxygen and metal ion. In addition, the bonding prevented metal ions from falling down the current collector, resulting in the better stability than graphite as a current collector.

Figure 3.9a showed an obviously low loss of capacitance about 10% after 10,000 charge/discharge process at 10 A g^{-1}. Further, the NC/CC//Mn/CC device exhibited the energy density and power density of 4.5 mWh cm^{-2} and 698.8 mW cm^{-2}, respectively, when tested in a two-electrode system (Figure 3.9b).

In summary, the unique concept of the controlled ratio between nickel ions and cobalt ions improved electrochemical performance and stability. In addition, the carbonized cotton provided the strong mechanical property treating with a pressure and the coordinate bond with metal ions, indicating that it has properties such as retained structure and higher stability than graphite. The NC/CC//Mn/CC was optimized by the simple fabrication and activation process.

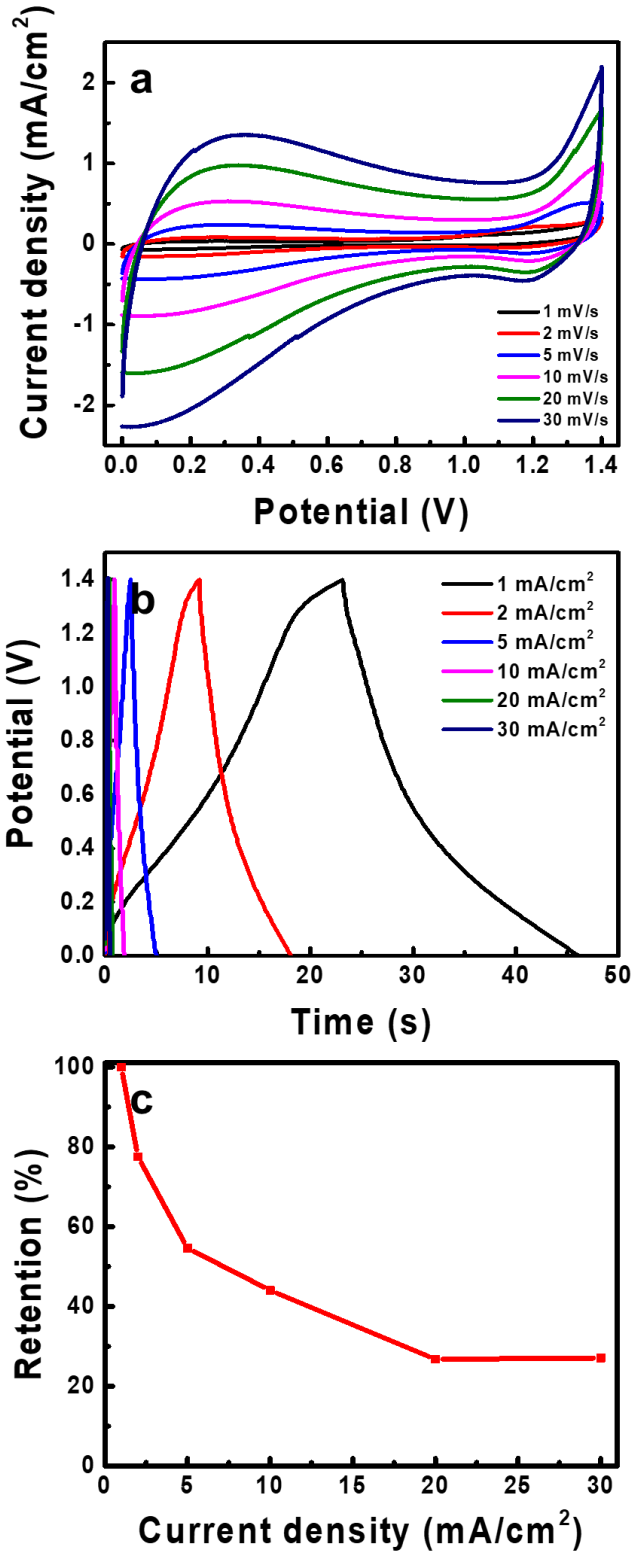

Figure 3. 7. Electrochemical performance of hybrid-capacitor: (a) CV curves, (b) GCD curves, and (c) Retention with increased current densities in a two-electrode system.

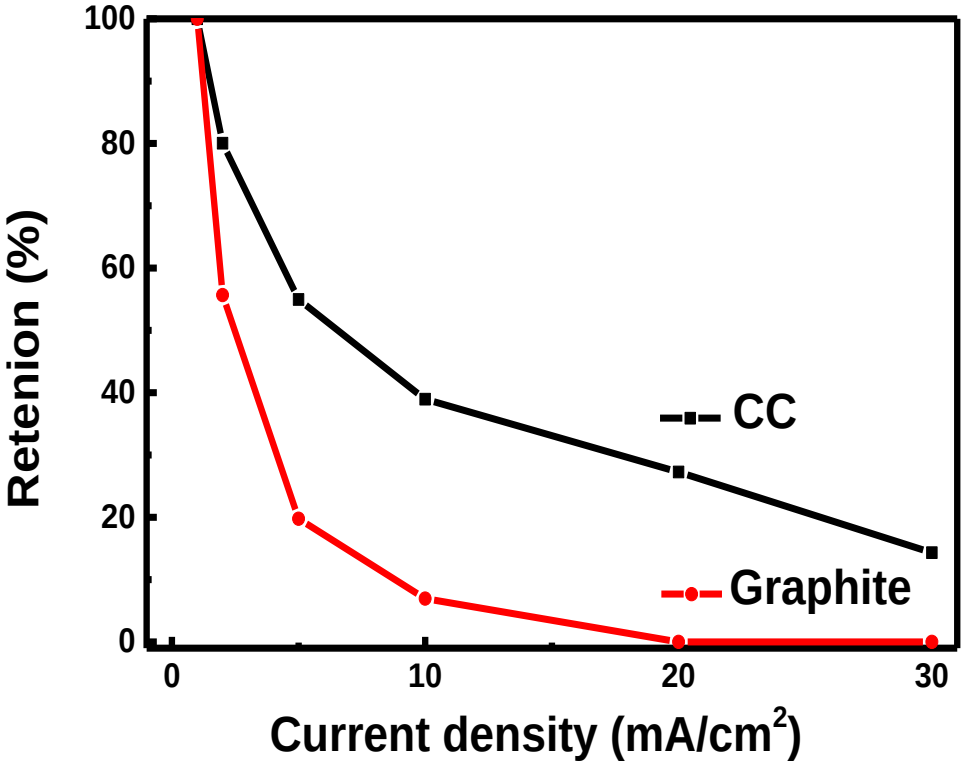

Figure 3. 8. Comparison of retention with the current collectors of CC and graphite.

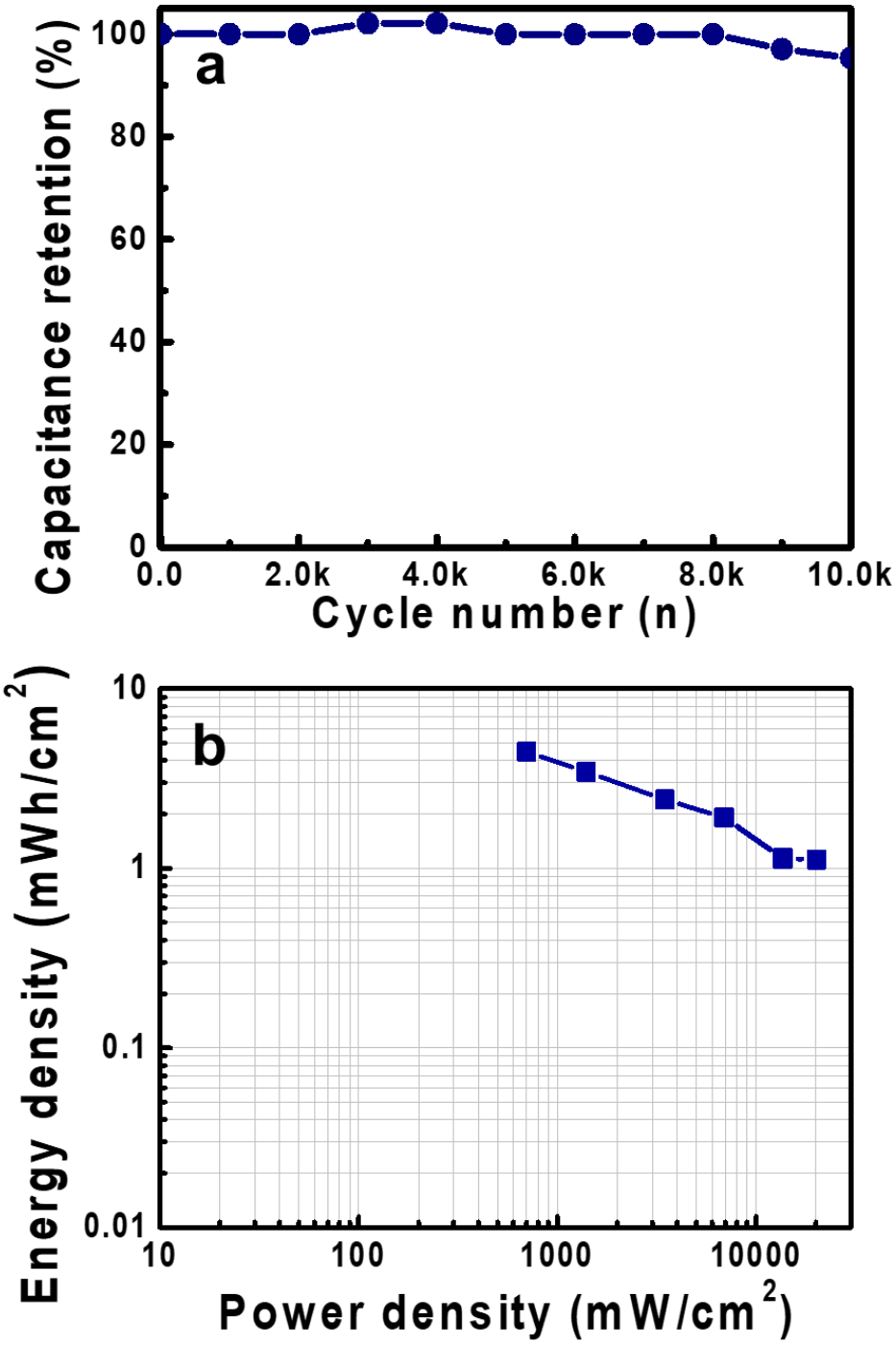

Figure 3. 9. Capacitor properties of the NC/CC//Mn/CC device: (a) Cycle stability for 10,000 cycles and (b) Ragone plot in a two-electrode system.

3.4 Conclusion

I have challenged a new concept for metal ion-colloid electrode as an active material to improve the electrochemical properties. A ratio of Ni^{2+} and Co^{2+} was controlled by the concentration of dip-coating solution to solve the problems in terms of the performance and stability for capacitor. The controlled electrode was performed to in situ activation process, forming the metal hydroxides to achieve the high capacitance. The prepared Ni^{2+}:Co^{2+} (1:1)-colloid electrode was used as a positive electrode with the Mn^{2+}-colloid electrode as a negative electrode. Furthermore, the O_2 plasma treated-carbonized cotton plays key role in retaining the stability with high current densities. For all these advantages, the NC/CC//Mn/CC device reached not only the stability of 27% while presenting the stability of 0% using graphite as a current collector but also retained the capacitance of about 90% at long cycle, respectively.

3.5 References

1. Tang, J.; Jin, M.; Yuan, P.; Fu, Y.; Ma, X., Large-area, ultrathin inorganic network coverages-graphene hierachical electrodes for flexible, heat-resistant energy storage application. *Adv. Energy Mater.* **2016,** *6*, 1600146.
2. Yao, B.; Huang, L.; Zhang, J.; Gao, X.; Wu, J.; Cheng, Y.; Xiao, X.; Wang, B.; Li, Y.; Zhou, J., Transparent molybdenum trioxide nanopaper for energy storage. *Adv. Mater.* **2016,** *28*, 6353-6358.
3. Bo, Z.; Zhu, W.; Ma, W.; Wen, Z.; Shuai, X.; Chen, J.; Yan, J.; Wang, Z.; Cen, K.; Feng, X., Verically oriented graphene bridging active-layer/current-collector interface for ultrahigh rate supercapacitors. *Adv. Mater.* **2013,** *25*, 5799-5806.
4. Simon, P.; Gogotsi, Y.; Dunn, B., Where do batteries end and supercapacitors begin? *Science* **2014,** *343*, 1210-1211.
5. Liu, C.; Yu, Z.; Neff, D.; Zhamu, A.; Jang, B. Z., Graphene-based supercapacitor with an ultrahigh energy density. *Nano Lett.* **2010,** *10*, 4863-4868.
6. Guan, C.; Liu, J.; Wang Y.; Mao, L.; Fan, Z.; Shen, Z.; Zhang, H.; Wang, J., Iron oxide-decorated carbon for supercapacitor anodes with ultrahigh energy density and outstanding cycling stability. *ACS Nano* **2015,** *9* (5), 5198-5207.
7. Zhu, Y. W.; Murali, S.; Stoller, M. D.; Ganesh, K. J.; Cai, W. W.; Ferreira, P. J.; Pirkle, A.; Wallace, R. M.; Cychosz, K. A.; Thommes, M.; Su, D.; Stach, E. A.; Ruoff, R. S., Carbon-based supercapacitors produced by activation of graphene. *Science* **2011,** *332* (6037), 1537-1541.
8. Lee, J. S.; Kim, S. I.; Yoon, J. C.; Jang, J. H., Chemical vapor deposition of mesoporous graphene nanoballs for supercapacitor. *Acs Nano* **2013,** *7* (7), 6047-6055.
9. Yoon, J. C.; Lee, J. S.; Kim, S. I.; Kim, K. H.; Jang, J. H., Three-dimensional graphene nano-networks with high quality and mass production capability via precursor-assisted chemical vapor deposition. *Sci. Rep-Uk* **2013,** *3*.
10. Ma, L. P.; Yang, Y., Solid-state supercapacitors for electronic device applications. *Appl. Phys. Lett.* **2005,** *87* (12).
11. Hung, K. S.; Masarapu, C.; Ko, T. H.; Wei, B. Q., Wide-temperature range operation supercapacitors from nanostructured activated carbon fabric. *J. Power Sources* **2009,** *193* (2), 944-949.
12. Conway, B. E., Transition from supercapacitor to battery behavior in electrochemical energy-storage. *J. Electrochem. Soc.* **1991,** *138* (6), 1539-1548.
13. Yu, M.; Lin, D.; Feng, H.; Zeng, Y.; Tong, Y.; Lu, X., Boosting the energy density of carbon-based aqueous supercapacitors by optimizing the surface charge. *Angew. Chem. Int. Ed.* **2017,** *56* (20), 5454-5459.
14. Choi, N.-S.; Chen, Z.; Freunberger, S. A.; Ji, X.; Sun, Y. K.; Amine, K.; Yushin, G.; Nazar, L. F.;

Cho, J.; Bruce, P. G., Challenges facing lithium batteries and electrical double-layer capacitors. *Angew. Chem. Int. Ed.* **2012,** *51* (40), 9994-10024.

15. Costentin, C.; Porter, T. R.; Saveant, J. M., How do pseudocapacitors store energy? Theoretical analysis and experimental illustration. *ACS Appl. Mater. Interfaces* **2017,** *9* (10), 8649-8658.
16. Augustyn, V.; Come, J.; Lowe, M. A.; Kim, J. W.; Taberna, P. L., Tolbert, S. H.; Abruna, H. D.; Simon, P.; Dunn, B., High-rate electrochemical energy storage through Li^+ intercalation pseudocapacitance. *Nat. Mater.* **2013,** *12* (6), 518-522.
17. Hu, C. C.; Chang, K. H.; Lin, M. C.; Wu, Y. T., Design and tailoring of the nanotubular arrayed architecture of hydrous RuO2 for next generation supercapacitors. *Nano Lett.* **2006,** *6* (12), 2690-2695.
18. Qu, Q. T.; Zhang, P.; Wang, B.; Chen, Y. H.; Tian, S.; Wu, Y. P.; Holze, R., Electrochemical performance of MnO_2 nanorods in neutral aqueous electrolytes as a cathode for asymmetric supercapacitors. *J. Phys. Chem. C* **2009,** *113* (31), 14020-14027.
19. Rustomji, C. S.; Yang, Y.; Kim, T, K.; Mac, J.; Kim, Y. J.; Caldwell, E.; Chung, H.; Meng, Y. S., Liquefied gas electrolytes for electrochemical energy storage devices. *Science* **2017,** *356*, I4263.
20. Mourad, E.; Coustan, L.; Lannelonque, P.; Zigah, D.; Mehdi, A.; Vioux, A.; Freunberger, S. A.; Favier, F.; Fontaine, O., Biredox ionic liquids with solid-like redox density in the liquid state for high-energy supercapacitors. *Nat. Mater.* **2017,** *16* (4), 446-453.
21. Chen, K.; Xue, D., Colloidal supercapacitor electrode materials. *Mater. Res. Bull.* **2016,** *83*, 201-206.
22. Chen, K.; Xue, D., Rare earth and transitional metal colloidal supercapacitors. *Sci. China Technol. Sci.* **2015,** *58*, 1768-1778.
23. Chen, K.; Yang, Y.; Li, K.; Ma, Z.; Zhou, Y.; Xue, D., $CoCl_2$ designed as excellent pseudocapacitor electrode materials. *ACS Sustainable Chem. Eng.* **2014,** *2*, 440-444.
24. Liang, X.; Chen, K.; Xue, D., A flexible and ultrahigh energy density capacitor via enhancing surface/interface of carbon cloth supported colloids. *Adv. Energy Mater.* **2018,** *8*, 1703329.
25. Chen, K.; Xue, D., *In situ* electrochemical activation of Ni-based colloids from from an NiCl2 electrode and their advanced energy storage performance. *Nanoscale* **2016,** *8*, 17090-17095.
26. Chen, K.; Xue, D., pH-Assited crystaliation of Cu_2O: Chemical reactions control the evolution from nanowires to polyhedra. *CrystEngComm.* **2012,** *14*, 8068-8075.
27. Chen, K.; Xue, D.; Komarneni, S., Colloidal pseudocapacitor: Nanoscale aggregation of Mn colloids from $MnCl_2$ under alkaline condition. *J. Power Sources* **2015,** *279*, 365-371.
28. Lu, P.; Liu, F.; Xue, D.; Yang, H.; Liu, Y., Phase selective route to $Ni(OH)_2$ with enhanced supercapacitance: Performance dependent hydrolysis of $Ni(Ac)_2$ at hydrothermal conditions. *Electrochim. Acta* **2012,** *78*, 1-10.

29. Cao, L.; Xu, F.; Liang, Y.; Li, H., Preparation of the novel nanocomposite $Co(OH)_2$/ultra-stable Y zeolite and its application as a supercapacitor with high energy density. *Adv. Mater.* **2004,** *16*, 1853-1857.

30. Yan, J.; Fan, Z.; Sun, W.; Ning, G.; Wei, T.; Zhang, Q.; Zhang, R.; Zhi, L.; Wei, F., Advanced asymmetric supercapacitors based on $Ni(OH)_2$/graphene and porous graphene electrodes with high energy density. *Adv. Funct. Mater.* **2012,** *22*, 2632-2641.

31. Conway, B. E., Electrochemical supercapacitors: Scientific fundmentals and technological applications; Kluwer-Academic: New York **1999**.

Publication list

1. Jongha Hwang, Sun-I Kim, Jong-Chul Yoon, Seong-Ji Ha, and Ji-Hyun Jang*, Realizing battery-like energy density with asymmetric supercapacitors achieved by using highly conductive three-dimensional graphene current collectors, J. Mater. Chem. A **2017**, *5*, 13347-13356.

Acknowledgment

유니스트에서의 석사 생활을 마무리하면서 저에게 많은 도움을 주신 분들께 감사하다는 말을 전하고 싶습니다. 우선, 저를 항상 응원해주시고 지켜봐 주신 부모님께 가장 먼저 감사하다는 말을 전하고 싶습니다. 그리고 부족했던 제가 석사 생활을 하면서 성장하는데 도움을 주신 장지현 교수님께 많은 것을 배우는 기회를 주셔서 감사하다고 전해드리고 싶습니다. 또한, 바쁘신 와중에도 졸업 논문 심사에 참여하여 많은 조언해주신 박종남 교수님, 송현곤 교수님께도 감사드립니다. 마지막으로는 대학원 생활을 함께한 우리 실험실 사람들에게 고마움을 전하고 싶습니다. 실험실에 잘 적응할 수 있게 여러모로 도와주고 잘 모르는 부분에 대해서도 한번도 화내지 않고 꼼꼼하게 알려준 종하오빠에게 가장 큰 고마움을 전하고 싶습니다. 때로는 친오빠처럼 때로는 사수처럼 따뜻하게 저를 대해줘서 대학원 생활에서의 좋은 추억으로 남을 수 있게 해주어서 고맙습니다. 또한, 선이 언니, 광현 오빠, 성욱 오빠, 익희 오빠, 종철 오빠, 기용 오빠, 명준 오빠, 지훈 오빠, 진욱 오빠, 철원이, 재은이, 주형이, 세영이, 수희 모두에게 실험실 생활을 함께 해준 것에 대해 감사함을 전합니다. 석사 학위를 잘 마무리할 수 있게 도움을 주신 많은 분들, 다시 한번 더 감사드리고 항상 건강하시기 바랍니다.